BRNO UNIVERSITY OF TECHNOLOGY

Faculty of Mechanical Engineering

MASTER'S THESIS

Brno, 2018   Bc. Jana Midlíková

BRNO UNIVERSITY OF TECHNOLOGY

VYSOKÉ UČENÍ TECHNICKÉ V BRNĚ

FACULTY OF MECHANICAL ENGINEERING

FAKULTA STROJNÍHO INŽENÝRSTVÍ

INSTITUTE OF PHYSICAL ENGINEERING

ÚSTAV FYZIKÁLNÍHO INŽENÝRSTVÍ

DESIGN OF THE FAR-INFRARED SPECTROMETER COUPLING TO A SUPERCONDUCTIVE MAGNET AND MAGNETO-OPTICAL MEASUREMENTS IN THE FAR-INFRARED REGION

NÁVRH PROPOJENÍ FAR-INFRARED SPEKTROMETRU K SUPRAVODIVÉMU MAGNETU A MAGNETO-OPTICKÉ MĚŘENÍ VE FAR-INFRARED OBLASTI

MASTER'S THESIS

DIPLOMOVÁ PRÁCE

AUTHOR   Bc. Jana Midlíková
AUTOR PRÁCE

SUPERVISOR   Ing. Petr Neugebauer, Ph.D.
VEDOUCÍ PRÁCE

BRNO 2018

Specification Master's Thesis

Department: Institute of Physical Engineering
Student: **Bc. Jana Midlíková**
Study programme: Applied Sciences in Engineering
Study branch: Physical Engineering and Nanotechnology
Leader: **Ing. Petr Neugebauer, Ph.D.**
Academic year: 2017/18

Pursuant to Act no. 111/1998 concerning universities and the BUT study and examination rules, you have been assigned the following topic by the institute director Master's Thesis:

Design of the far–infrared spectrometer coupling to a superconductive magnet and magneto–optical measurements in the far–infrared region

Concise characteristic of the task:

Far–infrared spectroscopy in high magnetic fields presents an ideal combination of experimental techniques that can probe and elucidate properties of the most advanced materials. This technique provides complementary information to the commonly used measurements of transport, magnetization, and thermodynamic properties. In the diploma thesis a device based on far–infrared spectroscopy in magnetic field will be designed. The device will be tested by magneto–optical measurement of selected molecular magnets or similar compounds in far–infrared region.

Goals Master's Thesis:

1. To elaborate a search study on far–infrared spectroscopy, molecular magnetism and existing aconnecting spectrometer to a magnet.
2. To propose a design solution for coupling of far–infrared spectrometer to a superconductive magnet and to design a beam propagation in this device.
3. To measure the magneto–optical properties of selected molecular magnets.

Recommended bibliography:

GRIFFITHS, P. R., DE HASETH, J. A.: Fourier Transform Infrared Spectrometry. Chemical Analysis: A Series of Monographs on Analytical Chemistry and Its Applications. Wiley, 2007. ISBN 9780470106297.

KÜHNE, P., HERZINGER, C. M., et al.: Invited Article: An integrated mid-infrared, far-infrared, and terahertz optical Hall effect instrument. Review of Scientific Instruments. American Institute of Physics, 1407, 85(7). ISSN 0034-6748.

PADILLA, W. J., BASOV, D. N., et al.: Broadband multi-interferometer spectroscopy in high magnetic fields: From THz to visible. Review of Scientific Instruments. American Institute of Physics. 75(11), 4710-4717. ISSN 0034-6748.

TAKEHANA, K., OSHIKIRI, M., et al.: Far-infrared spectroscopy in high magnetic fields. Physica B: Physics of Condensed Matter. Elsevier B.V, 1996, 216(3), 354-357. ISSN 0921-4526.

Deadline for submission Master's Thesis is given by the Schedule of the Academic year 2017/18

In Brno,

L. S.

....
prof. RNDr. Tomáš Šikola, CSc.
Director of the Institute

....
doc. Ing. Jaroslav Katolický, Ph.D.
FME dean

Abstract

The thesis deals with the development of the far-infrared (FIR) spectroscopy in the high magnetic field. The combination of the FIR spectroscopy and high magnetic field is a very important tool in the characterization of materials such as Single-Molecule Magnets (SMMs). It also presents an ideal experimental technique that can probe and elucidate properties of novel 2D materials. The FIR spectroscopy in the magnetic field also allows studying Electron Paramagnetic Resonance (EPR) of SMMs with very large zero-field splitting, mainly based on transition metal complexes or lanthanides, in which commonly used EPR systems do not provide experimental access to the magnetic resonance transitions. In the thesis, two setups of the FIR spectrometers coupled to the superconductive magnets are described in detail. The first described setup, located at the University of Stuttgart, is already assembled and its performance is discussed. The magneto-optical measurements of SMMs performed on this setup are presented. The second magneto-optical setup draws on the experiences gained in the first setup and is designed for CEITEC.

Keywords

Single-Molecule Magnets, far-infrared spectroscopy, high magnetic field, magneto-optical setup, electron paramagnetic resonance

Abstrakt

Práca sa zaoberá vývojom ďalekej infračervenej spektroskopie v silnom magnetickom poli. Kombinácia ďalekej infračervenej spektroskopie a silného magnetického poľa je veľmi dôležitým nástrojom pri charakterizácii materiálov, ako sú jedno-molekulové magnety. Predstavuje tiež ideálnu experimentálnu techniku, ktorá dokáže skúmať a objasniť vlastnosti nových 2D materiálov. Ďaleká infračervená spektroskopia v magnetickom poli taktiež umožňuje študovať elektrónovú paramagnetickú rezonanciu (EPR) jedno-molekulových magnetov s veľmi veľkým delením pri nulovom poli, hlavne na báze komplexov prechodných kovov alebo lantanoidov, v ktorých bežne používané EPR systémy neposkytujú experimentálny prístup k magnetickým rezonančným prechodom. V práci sú podrobne popísané dve zostavy ďaleko infračervených spektrometrov pripojené k supravodivým magnetom. Prvá opísaná zostava, ktoré sa nachádza na univerzite v Stuttgarte, je už zmontovaná a jej výkon je diskutovaný. Magneto-optické merania jedno-molekulových magnetov vykonané na tejto zostave sú predstavené. Druhá magneto-optická zostava čerpá zo skúseností získaných pri prvej zostave a je určená pre CEITEC.

Klíčová slova

jedno-molekulové magnety, ďaleká infračervená spektroskopia, silné magnetické pole, magneto-optická zostava, elektrónová paramagnetická rezonancia

Declaration

I declare that I have elaborated my master's thesis on the theme of "Design of the far-infrared spectrometer coupling to a superconductive magnet and magneto-optical measurements in the far-infrared region" independently, under the supervision of the master's thesis supervisor and with the use of technical literature and other sources of information which are all quoted in the thesis and detailed in the list of literature at the end of the thesis.

As the author of the master's thesis, I have not infringed any copyright. In particular, I have not unlawfully encroached on anyone's personal copyright and I am fully aware of the consequences in the case of breaking Regulation §11 and the following of the Copyright Act No 121/2000 Vol., including the possible consequences of criminal law resulted from Regulation §152 of Criminal Act No 140/1961 Vol.

Brno   . . . .
                                                                (author's signature)

Acknowledgement

Bc. Jana Midlíková

Dedicated to the memory of my beloved father

Ján Midlík

Contents

Introduction

Nowadays, we live in the digital era when the growing need for smaller and more energy efficient devices has made higher density data storage one of the most important technological quests. Any improvement in data storage and energy efficiency could also have a huge impact on data centers around the world which consume a lot of energy to store a high amount of data. Recently, estimate survey has shown that the total amount of data stored worldwide is about to rise from 4.4 trillion gigabytes in 2013 to 44 trillion gigabytes by 2020 [1]. Therefore, research is currently focused on developing denser means of data storage that can store greater amounts of data in a more energy efficient way. The key research topics involve working at the level of individual atoms and molecules, representing the ultimate limit of technological miniaturization [2].

With dimensions close to a nanometer and the ability to store one bit of information, molecules that possess bistable magnetization called Single-Molecule Magnets (SMMs) give a possibility to move technology forward. Their potential applications in the storage and processing of digital information have drawn an attention of scientific community over the past two decades. The molecular nature of these materials offers unique attributes that may allow information to be stored at much higher densities and remarkable speeds.

This thesis deals with the development of the far-infrared (FIR) spectroscopy in a high magnetic field. The combination of the FIR spectroscopy and the high magnetic field is a very important tool in the characterization of SMMs although, it is not limited to this application. It also presents an ideal experimental technique that can probe and elucidate properties of novel materials, such as 2D materials. Since (FIR) energy region in high magnetic field covers the magnetic resonances, this method allows to study Electron Paramagnetic Resonance (EPR) by the use of FIR region and thus broaden a typical microwave range for investigation of SMMs.

The aim of this master's thesis is elaborating a research study on molecular magnetism, far-infrared spectroscopy and existing devices connecting spectrometer to a magnet, proposal of a design solution for coupling of the far-infrared spectrometer to a superconductive magnet and the design of a beam propagation in this device and last but not least, measurements of the magneto-optical properties of selected molecular magnets.

This thesis is divided into several parts. The first part is theoretical and consists of the first two chapters. The first chapter introduces molecular magnetism and then focuses mainly on SMMs, their interesting properties, promising applications and current challenges, and a special group of lanthanide SMMs. At the end of this chapter, a brief introduction to EPR spectroscopy – a powerful spectroscopic method

for investigation of SMMs – is presented. Then follows the second chapter, which is devoted to Far-Infrared (FIR) Spectroscopy its history, and theoretical background. Additionally, essential components of typical Fourier Transform Infrared Spectrometer (FT-IR) are described here. Finally, FIR spectroscopy in the high magnetic field and existing magneto-optical setups worldwide are presented.

The second part of the thesis (Chapter 3) is practical, dedicated to the design of the magneto-optical setups. The first described setup was designed during my internship at the University of Stuttgart in Germany at Institute of Physical Chemistry (IPC). The second described setup is designed for Central European Institute of Technology (CEITEC).

The last part of the thesis (Chapter 4) is experimental and provides magneto-optical measurements on two different setups. The first described FIR measurements were performed on the already assembled magneto-optical setup at IPC in Stuttgart (Germany). Moreover, the performance of this setup is discussed here. The second described FIR measurements were carried out at Grenoble High Magnetic Field Laboratory (GHMFL) at French National Center for Scientific Research (CNRS). By these measurements, the importance of the FIR spectroscopy in the high magnetic field method in the field of molecular magnetism is demonstrated and explained.

1 Molecular Magnetism

The last years have seen an explosive increasing interest in the search for molecular species with unusual magnetic properties which could lead to molecular devices. Therefore, the development of molecular magnetism is currently an important field of study in chemistry and physics.

Molecular magnetism can be defined as an interdisciplinary field including chemistry, physics and materials science dealing with the design, the synthesis, and the characterization of molecular based magnetic materials. It is a relatively young scientific field which owes much to the great progress made in the second half of the 20th century. Essential ingredients for the birth and the development of this new field were mainly a deeper understanding of the magnetic phenomena in the condensed matter and an ability to manipulate molecules [3].

A particularly appealing area in molecular magnetism are molecules behaving as tiny magnets and thus known also as Single-Molecule Magnets (SMMs), sometimes called Molecular Nanomagnets (MNMs). SMMs are molecular species built up of a paramagnetic transition metal or lanthanide metal ions that exhibit borderline behavior between classical and quantum physics. They, on one hand, show magnetic hysteresis as ordinary magnets do and, on the other hand, they are small enough to show quantum effects. This combination of classical and quantum phenomena is very attractive from the theoretical point of view since it provides new challenging questions, but it can also bring many technological applications, especially in the fields of data storage, quantum computation, and spintronics. For example, they offer the possibility of storing information at the molecular level. The incorporation of SMMs into multifunctional materials is thus expected to become a very fruitful research area in the near future [3, 4]. The following section will be therefore dedicated to these molecular species, their brief history, interesting features, possible applications and current challenges.

1.1 Single-Molecule Magnets (SMMs)

In 1993, the fascinating discovery of slow relaxation of the magnetization at low temperature and hysteresis in a dodecanuclear manganese cluster called Mn_{12}[1] (Figure 1.1) 0was observed and then published in scientific journal Nature [5]. Hysteresis and slow relaxation of the magnetization is a well-known feature of bulk ferromagnets, so it was astonishing to observe these characteristics in a material that does not have a 3-dimensional magnetic structure. The Mn_{12} cluster acts as a tiny magnet so, for

---

[1]specifically $Mn_{12}O_{12}(CH_3COO)_{16}(H_{12}O)_4$

this reason, is considered as the first example of a today large family of magnetic materials known as SMMs. It consists of twelve manganese ions, four inner Mn^{3+} ions with spins pointing down and eight outer Mn^{4+} ions with spins pointing up that leads to a total spin of $S = 10$ in the direction of the Mn^{4+} ions at low temperatures (see Figure 1.1). In the following years, a wide variety of SMMs has been synthesized as well as Single-Ion Magnets (SIMs) – special subclass of SMMs composed of only one metal ion. In the beginning, they were primarily based on $3d$-transition metal ions like manganese, cobalt or iron. A well-known example of such SMMs besides the Mn_{12} is, for instance, the cluster Fe_8 [3,6].
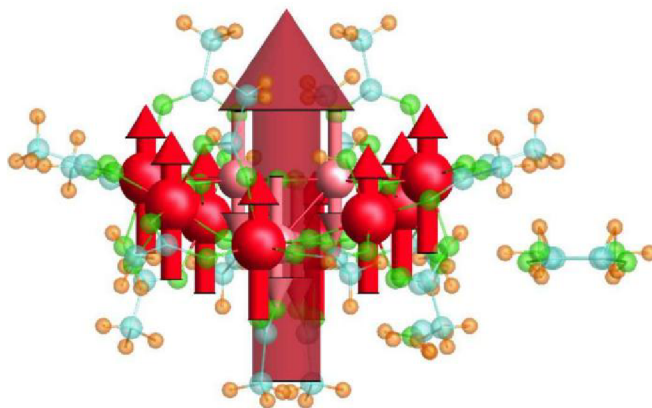
Figure 1.1: Molecular structure of $Mn_{12}O_{12}(CH_3COO)_{16}(H_{12}O)_4$. Four inner Mn^{3+} ions, each have a spin of S=3/2 pointing down (light pink) and eight outer Mn^{4+} ions, each have a spin S=2 pointing up (red). The spins of the cluster couple together to the total spin of S=10 (dark red) pointing in the direction of the Mn^{4+} ions. Adapted from [6].

1.1.1 Properties

SMMs are molecules that show slow relaxation of the magnetization of purely molecular origin [7]. This key feature, which basically describes the quality of SMMs, can be described in different ways. Commonly used characteristic quantities are the blocking temperature T_B and the effective energy barrier (also called anisotropy barrier) U_{eff} [6]. The blocking temperature can be defined as the temperature below which the relaxation of the magnetisation becomes slow compared to the time scale of a particular investigation technique[2] [8]. The anisotropy barrier is an energy

---

[2]for example, a molecule magnetized at 2 K retains 40% of its magnetization after 2 months, but by lowering the temperature to 1.5 K it would take 40 years to reach the same state [8]

barrier that the spins must overcome when they switch from a parallel alignment to an anti-parallel alignment so that, at low temperatures, the system is trapped in one of the high-spin energy wells (see Figure 1.2. This anisotropy barrier (U_{eff}) is for the systems such as $3d$-transition metal defined as

$$U_{eff} = S^2|D| \text{ for integer spin and } U_{eff} = (S^2 - 1/4)|D| \text{ for half-integer spin, } \quad (1.1)$$

where S is the spin of the ground state (total spin) and D is the magnetic anisotropy constant, more precisely, the axial term of the second rank Zero-Field Splitting (ZFS) tensor measured in wavenumbers, which will be explained further. Parameter D is for SMMs negative, therefore only its absolute value is considered in the equation. The barrier U_{eff} is usually reported in cm^{-1} or in kelvins (K). The higher the barrier, the longer a material remains magnetized, therefore U_{eff} should be as large as possible [9,10]. In case of the Mn$_{12}$ cluster with the total spin $S = 10$ (involving 20 unpaired electrons), and $D = -0.51\,\mathrm{cm}^{-1}$, the energy barrier is $U_{eff} = 51\,\mathrm{cm}^{-1}$ (equivalent to 60 K) [11].

The magnetic behaviour of SMMs is governed by the anisotropic zero-field splitting (ZFS) parameters, D and E, according to the following zero-field spin Hamiltonian:

$$\hat{\mathcal{H}} = D\hat{S}_z^2 + E(\hat{S}_x^2 - \hat{S}_y^2) = D[\hat{S}_z^2 - \frac{1}{3}S(S+1)] + E(\hat{S}_x^2 - \hat{S}_y^2), \quad (1.2)$$

where D and E are the axial and rhombic zero-field splitting parameters, respectively. $\hat{S}$ is a spin operator describing the spin projection along a given axis. Interaction of the electrons with the electric field generated by the surrounding atoms (i.e. the crystal field or ligand field) causes a splitting of the more than twofold (Kramers) degenerated ground state of the electron system even in the absence of an external magnetic field – ZFS. The energy difference between Kramers doublets corresponds to the multiples of D (for $S = 3/2$ it is $2D$ in the absence of a rhombic ZFS term) [12,13].

The occurrence of the energy barrier is closely related to magnetic anisotropy, which is in case of SMMs the phenomenon that a molecule can be more easily magnetized along one direction than along another (along the so-called "Easy axis" rather than a plane perpendicular to Easy axis). It means that different orientations of the magnetic moment have different energies. In the absence of orbital angular momentum, which is the case of many transition metal ions, it is known as ZFS and the orientation of the magnetic moment is then characterized by the m_S quantum number. Since the second rank axial zero-field splitting D is for transition metal systems usually dominant, the potential energy has a parabolic dependence on m_S (see Figure 1.2 (a)). The discrete levels are a clear indication of the quantum nature

of the system. For a negative value D, it leads to an effective energy barrier U_{eff} (sometimes reffered as U), where for inverting of the magnetic moment, the system has to climb a number of steps on one side of the energy barrier and descend on the other [14]. Another definition of SMMs says that they are molecules which can be magnetized in a magnetic field and they will remain magnetized even after switching off the magnetic field. This is a property of the molecule itself and no interaction between the molecules is necessary for this phenomenon to occur. This feature makes SMMs fundamentally different from traditional bulk magnets [7].

The cluster Mn_{12} shows magnetic hysteresis as shown in Figure 1.2 (b). At zero magnetic field the magnetization can be either positive or negative, depending on the history of the sample, which means that SMMs are bistable [15]. A molecule with a bistable magnetization can be used for storing information, with one orientation of the magnetic moment encoding a binary 0, and the opposite orientation a binary 1. Therefore, the bistability of the magnetization of SMMs allows storage of information and can be utilised in magnetic data storage devices [16]. The magnetization in SMMs occurs due to the existence of a large energy barrier between the spin-up and spin-down states [9]. Their magnetization curves exhibit not only hysteresis, but also a step-like shape of the hysteresis loops (Figure 1.2 (b)), which arises from a phenomenon, occuring between the states on the opposite sides of barrier, known as Quantum Tunnelling of Magnetization (QTM) [17]. Such a quantum behaviour of magnetization can be in principle exploited for development of quantum computing [8].
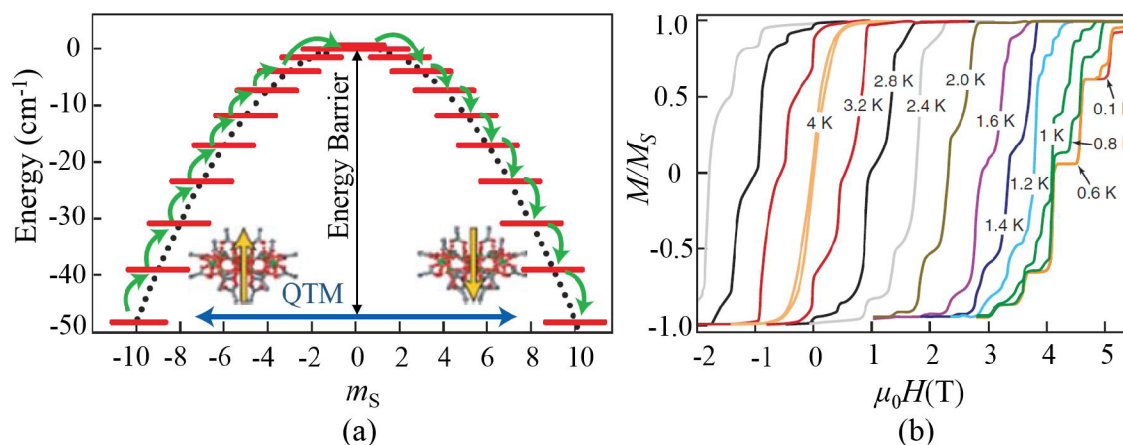

Figure 1.2: (a) Potential energy as a function of the m_s quantum number, calculated using ZFS parameters for Mn_{12}. (b) Hysteresis loop of Mn_{12} at different temperatures. The loops exhibit a series of steps due to QTM between energy levels. Adapted from [18].

For many years, research has focused on increasing the spin of the ground state S to obtain high energy anisotropy barrier U_{eff}, and therefore very slowly relaxing SMMs [16]. Nevertheless, further theoretical study demonstrated that large ground state spin S and large ZFS parameter D within one molecule could not be obtained simultaneously. With increasing S, D actually decreases and the energy barrier does not improve much [19]. For explanation of this fact, there is the article "A Criterion for the Anisotropy Barrier in Single-Molecule Magnets" from Oliver Waldman [20] and a theoretical study entitled "What is not needed to make a single-molecule magnet" from Neese and Pantazis [21]. Since 2003, considerable attention has thus increasingly focused on the elements with large magnetic anisotropies, especially lanthanides [10]. Next subsection will provide deeper insight into the problematics of lanthanides, because they are undoubtedly crucial in the field of molecular magnetism nowadays.

1.1.2 Lanthanides

For determining the properties of the building blocks in the periodic table (see Figure 1.3), it is convenient to use the magnetic orbitals, which are of p, d, and f nature. It is well known that p orbitals are external and reactive. Contrary to p orbitals, f orbitals are internal ones and very unreactive. In the middle are the d orbitals. The d orbitals play a fundamental role in the field of molecular magnetism because their intrinsic features combined with the versatile chemistry of transition metals offer a wide range of unusual magnetic properties. At the beginning of the molecular magnetism era, the choice was for the p orbitals followed by d orbitals and the f orbitals were neglected, but in the last few years f-block elements are intensively investigated for their attractive properties [22].

The lanthanides (or lantanoids) are the f-block elements of the periodic table with atomic numbers ranging from 57 to 71 from Lanthanum (La) to Lutetium (Lu), in which the 4f-shell is filled with electrons. These 15 elements are also referred to as Rare Earth Elements (REEs) (with inclusion of Scandium (Sc) and Yttrium (Y)) shown in Figure 1.3. The REEs share similar chemical properties and can be found in the same ore deposits. These elements exhibit special magnetic properties which arise from the electrons in the their unclosed and well shielded $4f$-shell [6].

Lanthanides play an important role in MM due to their usually large magnetic moments and large magnetic anisotropies compared to transition metals. A breakthrough of lanthanides in the field of molecular magnetism was the observation of slow relaxation of the magnetization in a phthalocyanine double-decker complex $[Pc_2Tb]^-TBA^+$, the first single-ion magnet, by Ishikawa et al. in 2003 [24]. The discovery not only boosted the research of lanthanide-based materials, it was also

Figure 1.3: Periodic table of the elements. Adapted from [23].

the starting point for the upcoming approach to search for SMMs on the single-ion level. Nowadays, most known single-ion based SMMs, also called SIMs, are based on lanthanide ions, but also transition metal based SIMs were discovered, based on e.g., cobalt or iron [6].

The anisotropy barrier of single lanthanide ions often lies in the range of a few hundred wavenumbers (with a record anisotropy barrier of $U_{eff} = 652\,\mathrm{cm}^{-1}$ in a heteroleptic bisphthalocyanine complex [10, 25]). On the contrary, the highest anisotropy barrier in transition metal ions is claimed for the cobalt complex with $U_{eff} = 67\,\mathrm{cm}^{-1}$ [10].

Regarding the applications of REEs, lanthanides are in high demand especially in the permanent magnet industry due to their strength, heat resistance, and ability to maintain their magnetism over very long periods. Magnets made from REEs elements such as neodymium or dysprosium are the strongest known permanent magnets. One of the key features that determine this excellent behaviour is their large magnetic anisotropy. Their higher performance and smaller size enables many miniature applications, such as personal electronic devices (smart phones, MP3 music players), for example a miniature magnet made with neodymium causes vibration of the cell phone [22]. Another example is the iPhone from Apple Inc. which uses eight REEs for the color screen, phone circuitry, speakers and the vibration unit. Basically, current modern technology cannot be imagined without REEs [6].

To sum up, SMMs based on f-elements, particularly those of the lanthanides, have accounted for some of the most eye-catching recent advances in molecular magnetism [26–28]. It may be even more important that Lanthanide SMMs (Ln-SMMs) have already shown considerable potential to be developed for surface deposition and device applications [10]. In addition, in 2017 the research team from the University of Manchester has reported in the Nature [29] a great achievement of magnetic hysteresis in SMMs at $-213\,°C$, which is only $17\,°C$ away from the temperature of liquid nitrogen, using a new molecule based on the REE – dysprosocenium [2].

1.1.3   Applications and Challenges

In the past two decades, molecular magnetism has caught the attention of condensed matter scientists because of the possible technological and industrial applications. They are looking for new materials to expand the current demand on data storage and computing. With the possibility of using spin flips for binary systems, molecular data storage and quantum computing have SMMs an opportunity to move technology forward. The molecular nature of SMMs offers unique attributes that allow to store information with much higher density and process them at unprecedented speeds [30]. Ultimately, new SMMs applications are expected, including the development of molecular spintronics [10, 31].

A stable magnetic moment can be used to store information at a molecular level. For a typical crystal with unit cell parameters of $1.5\,nm$, one can calculate[3] a two-dimensional data density of almost $300\,Tbit$ per in^2. In contrary to current hard disk models using single-domain magnetic particles, they are reaching around $1.2\,Tbit$ per in^2 [14, 32]. Magnetic data storage technologies, used in traditional hard disks (a typical example of hard disk drive (HDD) with its main parts is shown in Figure 1.4) with spinning platters, are built using "top-down" methods that involve making thin layers from a large piece of ferromagnetic material. This material contains many magnetic domains that are used to hold data and each of these magnetic domains is made of a large collection of magnetized atoms, whose magnetic polarity is set by the read/write head to represent data as either a binary one or zero. However, there is also an alternative "bottom-up" method which involves constructing storage devices by placing individual atoms or molecules one by one, each capable of storing a single bit of information. Due to communication between groups of neighboring magnetized atoms, magnetic domains retain their magnetic memory.

On the contrary, SMMs do not require this communication with their neighbors to retain their magnetic memory because their memory effect arises from quantum mechanics. Atoms or molecules are much smaller than the magnetic domains

---

[3] $\frac{(1 \text{ inch [m])}^2}{(\text{unit cell parameter [m])}^2} = \frac{(2.54 \times 10^{-2})^2}{(15 \times 10^{-10})^2} = 2.87 \times 10^{14} = 287\,\text{Tbit/in}^2$

currently used and they can be used individually rather than in groups. Therefore, they can be packed more closely together resulting in an enormous increase in data density. Such magnetic memory effects in SMMs were first demonstrated in 1993, and similar effects for single-atom magnets were shown in 2016 [2].

spinning platter

actuator

spindle
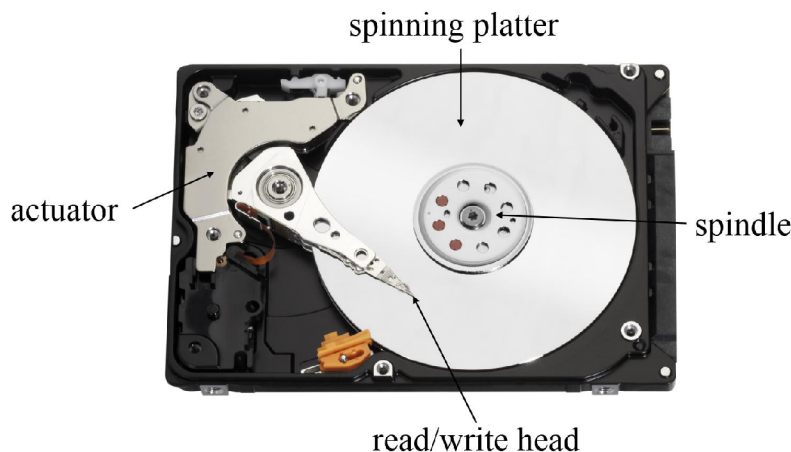
read/write head

Figure 1.4: Hard Disk Drive (HDD) from Western Digital designed for laptops and mobile applications with capacity 500 GB and 2.5 Inch form factor depicted with main parts: spinning platter, read/write head, actuator, spindle [33].

However, SMMs-based technology can only be realized when two major problems have been solved. The main problem standing in the way of moving these technologies out of the lab is that the unique properties of SMMs are currently only accessible using low temperatures; they do not work at room temperature yet. They require cooling with expensive and limited resource – liquid helium at the temperature of $-269\,°C$ (4 K). Therefore, either the operating temperatures need to rise significantly, or applications so novel need to be discovered that the temperature will no longer be a problem [2, 10].

Over the last 25 years there has been a big effort of scientific community to increase this temperature at which magnetic hysteresis — a demonstration of the magnetic memory effect – can be observed, to $-196\,°C$ (77 K). This temperature can be achieved with liquid nitrogen, which is abundant and cheap. Nevertheless, scientific development is getting close to the milestone with the REE molecule dysprosocenium [29], in which the research team from Manchester achieved magnetic hysteresis at $-213\,°C$ (only $17\,°C$ away from the temperature of liquid nitrogen), as stated previously. Another problem of SMMs is that the application of individual molecules on the surfaces was examined with just a few examples. Therefore, one of the greatest challenges in this field is to design and synthesize efficient SMMs that operate at temperatures likely to be of practical use, or which show physics that goes

beyond what can be achieved with conventional magnets [10]. Even though, there are other challenges in order to practically store individual bits of data. Demonstration of writing and non-destructively reading data in single atoms or molecules is crucial and ultimate test for this technologies. In 2017, it was for the first time achieved by a group of researchers at IBM who demonstrated the world's smallest magnetic memory storage device, built around a single atom [34].

Undoubtedly, the progress in fundamental science being made along the research of single-molecule storage devices is truly phenomenal. The synthetic chemistry techniques developed by groups working on SMMs allow designing molecules with customized magnetic properties, which will have applications in quantum computing and magnetic resonance imaging. Techniques for examination of their molecular and electronic properties will be mentioned below.

1.2 Spectroscopic Techniques

The main advantage of spectroscopic techniques in the study of single molecule magnets (SMMs) is their ability to probe molecular or electronic properties directly, as opposed to techniques that measure bulk properties such as magnetic susceptibility or magnetization. This allows much more accurate determination of parameters that control magnetic memory or QTM effects in SMMs. Such spectroscopic techniques are for example: Electron Paramagnetic Resonance (EPR), Nuclear Magnetic Resonance (NMR), Inelastic Neutron Scattering (INS) and Magnetic Circular Dichroism (MCD) spectroscopies. For purpose of this thesis, the most important technique is EPR Spectroscopy. It uses the resonant absorption of usually microwave (MW) radiation by paramagnetic molecules or ions with at least one unpaired electron spin in the presence of a static magnetic field [4]. Next subsection is thus dedicated to the brief overview of this method.

1.2.1 Electron Paramagnetic Resonance

Electron Paramagnetic Resonance (EPR) or Electron Spin Resonance (ESR) spectroscopy plays a crucial role in the determination of the physical and chemical properties and in explaining the origin of the unique behaviour of SMMs, i.e. the slow relaxation of the magnetization at low temperature and the observation of QTM [35]. This technique was also one of the first spectroscopic techniques used for probing the electronic and therefore magnetic structure of SMMs directly [4]. EPR is a powerful technique for for studying magnetic and electronic properties of materials with unpaired electrons[4], such as paramagnetic complexes, radicals or defects in crys-

---

[4]paramagnetic materials

tals [37].The basic concept of EPR spectroscopy is similar to NMR spectroscopy except electron spins are excited, instead of the spins of atomic nuclei. In the following, a brief introduction to the theory of EPR is presented.

An electron in an atom[5] has angular momentum called orbital angular momentum $\vec{L}$ with which an orbital magnetic dipole moment $\vec{\mu}_{orb}$ is associated:

$$\vec{\mu}_{orb} = -\frac{e}{2m}\vec{L}. \tag{1.3}$$

Neither $\vec{L}$ nor $\vec{\mu}_{orb}$ can be directly measured. Their components, which are quantized along a given axis (assume z axis) can be measured. Component L_z is determined by

$$L_z = m_l\hbar, \tag{1.4}$$

where m_l is the orbital magnetic number. The magnitude of $\vec{L}$ of an electron trapped in atom has quantized values given by

$$L = \sqrt{l(l+1)}\hbar, \tag{1.5}$$

where l is the orbital quantum number and $\hbar$ is reduced Planck constant[6] ($\hbar = h/2\pi$).

Every electron, whether in an atom or free, has an intrinsic angular momentum called spin angular momentum (or simply spin) $\vec{S}$ and intrinsic spin magnetic moment $\vec{\mu}_s$, which is proportional to $\vec{S}$. The magnitude S of $\vec{S}$ is quantized as

$$S = \sqrt{s(s+1)}\hbar, \tag{1.6}$$

where s is the spin quantum number and for electron is $s = \frac{1}{2}$. Spin $\vec{S}$ itself, as well as $\vec{\mu}_s$ cannot be measured. But components of $\vec{S}$ and $\vec{\mu}_s$ can be measured and they are quantized. If the component of spin $\vec{S}$ is measured along the z axis, then the measured component S_z can have only the two values given by

$$S_z = m_s\hbar, \text{ for } m_s = \pm\frac{1}{2}, \tag{1.7}$$

where m_s is called the spin magnetic quantum number. When S_z is parallel to the z axis, m_s is $+\frac{1}{2}$ and the electron is said to be "spin up" and when S_z is antiparallel, m_s is $-\frac{1}{2}$ and the electron is said to be "spin down" [36]. For the free electron, the component μ_z of electron spin magnetic moment along the direction of the magnetic field B applied along the direction z is

$$\mu_z = -g_e\mu_B m_s, \tag{1.8}$$

---

[5]localized electron
[6]$h = 6.63 \times 10^{-34}$ J·s

where $g_e = 2.0023$ is the free-electron g-factor, μ_B is Bohr magneton[7] defined as $\mu_B = \frac{e\hbar}{2m_e}$ in which e is the elementary charge m_e is the mass of an electron.

The total magnetic moment $\vec{J}$ of a particle is composed of orbital momentum $\vec{L}$ and spin $\vec{S}$ by equation $\vec{J} = \vec{L} + \vec{S}$.

When an electron is placed in an external magnetic field B, the energy U associated with the orientation of the spin magnetic dipole moment is

$$U = -\vec{\mu_s} \cdot \vec{B} = -\mu_z B_{ext} = g_e \mu_B m_s B. \tag{1.9}$$

Since an unpaired electron has the two possible values of m_s, the energy of an electron in a magnetic field B can be either $U_{upper} = \frac{1}{2}g_e\mu_B B$ for $m_s = +1/2$ or $U_{lower} = -\frac{1}{2}g_e\mu_B B$ for $m_s = -1/2$. By varying the magnetic field B, it is possible to change the energy-level separation. The separation between the lower and the upper level (energy level splitting) in magnetic field is called Zeeman effect (sometimes called Zeeman splitting). The difference in energy between the two levels is

$$\Delta U = U_{upper} - U_{lower} = g_e\mu_B B. \tag{1.10}$$

It implies that for free unpaired electrons, the splitting of the energy levels is directly proportional to the magnetic field strength, as shown in Figure 1.5. Transitions between the two electronic Zeeman levels may be induced by an electromagnetic field of the appropriate frequency ν such that the photon energy $h\nu$ matches the energy-level separation ΔU [37]. This leads to the fundamental equation of EPR Spectroscopy where B designates the magnetic field that satisfies the resonance condition:

$$\Delta U = h\nu = g_e\mu_B B. \tag{1.11}$$

Commonly used microwave frequencies used in EPR are denoted as S-band (3.5 GHz), X-band (9.25 GHz), K-band (20 GHz), Q-band (35 GHz) and W-band (95 GHz) [38].

Like most spectroscopic techniques, EPR spectrometers measure the absorption of electromagnetic radiation. Such spectra are obtained by measuring the attenuation versus sweeping of the magnetic field. Lines or bands in a spectrum represent transitions between energy levels of the absorbing species and the frequency of each line or band measures the energy separation of two levels. The EPR spectrum is presented as a first-derivative of absorption spectrum (shown in Figure 1.5) for improved sensitivity [37].

---

[7]μ_B= 9.27×10^{-24} J/T
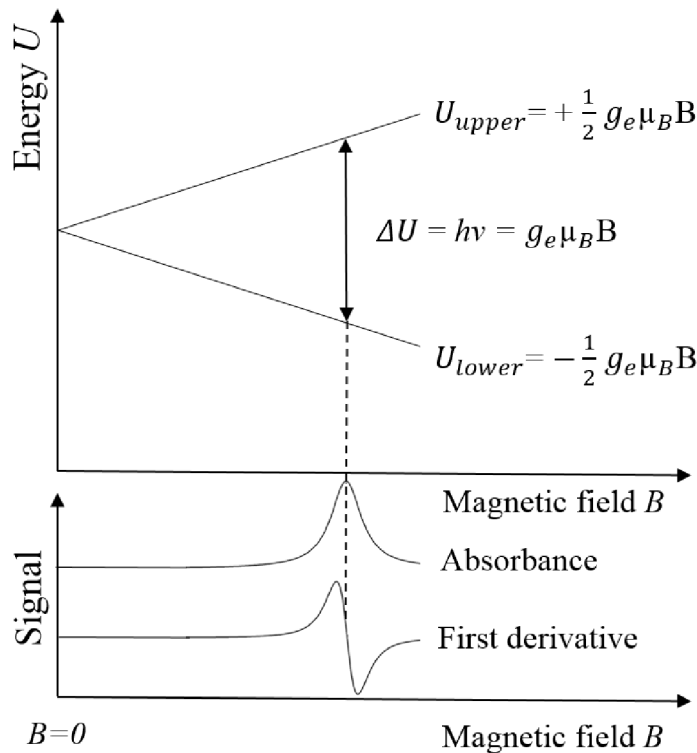
Figure 1.5: Splitting of electron spin states. Energy level diagram for a free electron in magnetic field B and the corresponding absorption spectrum and first derivative EPR spectrum.

1.2.2   EPR Spectrometer

There is a variety of EPR techniques. The most famous among them is continuous wave EPR (CW-EPR). In CW-EPR, the sample is subjected to a continuous beam of microwave irradiation of fixed frequency and the magnetic field is swept. In this sub-chapter will be described the principal components of a simple EPR spectrometer, specifically CW-EPR spectrometer [38]. In a CW-EPR spectrometer the microwave frequency is typically kept constant and the magnetic field is varied. This changes the separation of the energy levels, so that the condition of resonance is fulfilled when the difference of the energy levels participating in resonance becomes equal to $h\nu$. Such a spectrometer consists of four components:

- **A source of microwave radiation**, with components that measure and control the frequency and intensity of that radiation.
- **A magnetic field system**, which provides a stable, homogeneous and linearly varying magnetic field of arbitrary magnitude.
- **A cavity, or resonator**, system characterized by a fixed resonant frequency,

which holds the sample, controls and directs the microwave beam to and from the sample.

- **A signal - detection system**, which is accomplished by modulating the magnetic field by an alternating magnetic field, providing a sinusoidal voltage at the modulation frequency which is amplified as the useful EPR absorption signal for its recording. In the elementary system, the cavity can be avoided by simply placing the sample in the waveguide [9].

Historically, the vast majority of experiments have been carried out using CW spectrometers operating at the X-band frequency and employing conventional electromagnets. However, there have seen increasing development and applications of other EPR techniques such as High Frequency/Field EPR (HF-EPR), multifrequency EPR or Pulsed EPR in the last two decades. With the advent of HF-EPR spectrometers, EPR has today become a very sensitive and unique technique. This method uses microwaves of high frequency (typically hundreds of GHz) for the sample excitation [9]. For illustration, HF-EPR setup (shown in Figure 1.6) located at University of Stuttgart is presented in following text.

The tunable microwave source provides a radiation of frequencies: $\nu = 82 - 1100\,\text{GHz}$. For propagation of microwaves (MW) the spectrometer uses Quasi-Optics[8] (QO). The sample is located in a variable temperature insert (VTI), which provides temperature stabilization between $\text{T} = 1.8 - 300\,\text{K}$. VTI is put into a superconducting magnet capable of magnetic field up to $17\,\text{T}$. The microwave detection is provided by a InSb bolometer cooled by the liquid nitrogen and helium in order to increase its sensitivity [39].

---

[8]propagation of electromagnetic radiation when the size of the wavelength is comparable to the size of the optical components, it commonly describes the propagation of Gaussian beams where the beam width is comparable to the wavelength
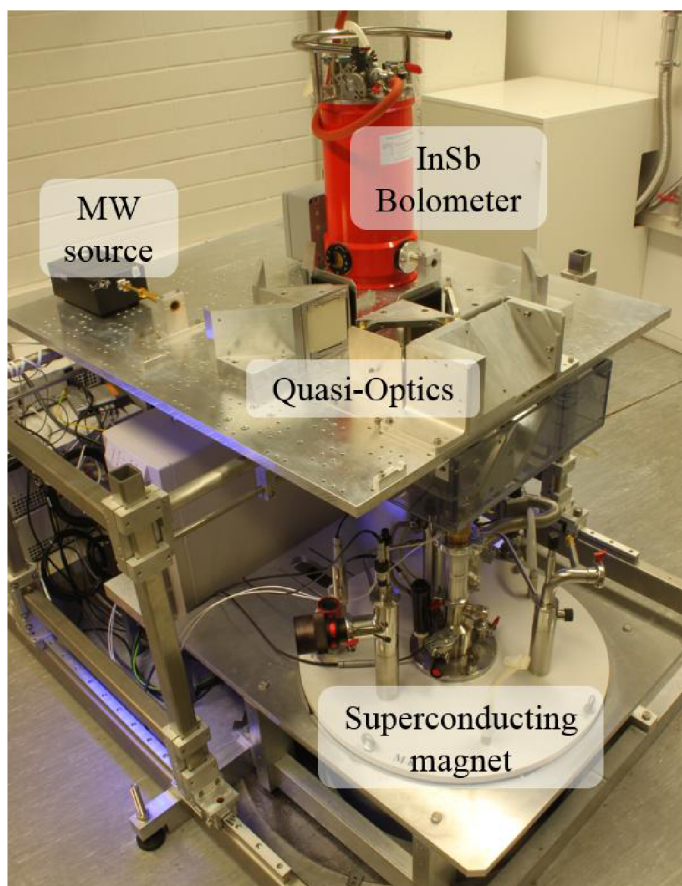
Figure 1.6: HF-EPR setup at University of Stuttgart

2   Far-Infrared Spectroscopy

Spectroscopy can be essentially defined as the study of the interaction of electromagnetic radiation with matter, which uses the result of this of this interaction to extract information. This thesis deals mainly with spectroscopy which studies interaction of infrared (IR) light with matter. Such a spectroscopy is called Infrared (IR) Spectroscopy and it is certainly one of the most important analytical technique available to scientists nowadays.

Infrared spectroscopy is also sometimes referred to as Fourier-Transform IR (FT-IR) Spectroscopy due to instruments used for measuring an infrared spectrum – FT-IR spectrometers. FT-IR or simply IR spectrometers (since almost all infrared spectra today are measured with these instruments) provide for measurement usually wide range of energies from ultraviolet (UV) to far-infrared (FIR) region. The thesis is focused especially on infrared spectroscopy in FIR region, therefore in the scope of whole thesis is commonly used the term FIR spectroscopy. The following subchapters are dedicated to: a brief history of how IR spectroscopy developed to FT-IR, definition of the IR radiation, introduction to IR Spectroscopy, FT-IR spectrometer and its basic components, Fourier Transformation, spectral analysis and at last, the FIR Spectroscopy in the high magnetic fields and existing devices.

2.1   From IR to FT-IR spectroscopy

The discovery of infrared radiation as a distinct region of the energy spectrum was made by the astronomer Sir William Herschel in 1800, when he measured the heating effect of sunlight. (He used just a prism and a mercury thermometer to record his observations of heat-based radiation beyond the range of the solar spectrum. However, IR spectroscopy could not develop at that time due to difficulties in building suitable detectors for measuring IR radiation. Since then a variety of methods have been used to improve the experimental techniques for measuring infrared spectra [40, 41].

First prototypes of IR spectrometers were built in the 1930s, that had increased interest in the potential of IR spectroscopy for analytical chemistry. Their commercial development quickly followed. Since 1940s, these spectrometers have been commercially available. At that time, the instruments relied on prisms to act as dispersive elements, but by the mid 1950s, diffraction gratings had been introduced [42]. In the middle of the 20th century, IR spectroscopy was established as a key analytical method in academic and industrial labs [40].

Nowadays, an integral part of IR spectroscopy is the use of FT-IR spectrometer which employs an interferometer and exploits the well-established mathematical

process of Fourier-transformation. History of the interferometers started almost a century ago, when Albert Michelson developed the interferometer for studying the speed of light and shortly after, Lord Rayleigh recognized that the output from an interferometer could be converted to a spectrum using a mathematical operation developed by the French mathematician Joseph Fourier in the 1820s. However, the lack of adequate computing power was the main reason that it took so many years for the instrument to utilize its full potential as an analytical tool. In 1964, the discovery of the Fast Fourier-Transform (FFT) algorithm by James Cooley and John Tukey reduced the time for the computer calculation of the transform from hours to just a few seconds [40].

A major breakthrough in infrared spectroscopy that led to the widespread use of infrared spectroscopy as a characterization tool was the introduction of the world's first commercial Fourier transform infrared spectrometer (MODEL FTS 14) by company Digilab in 1969. The combination of those discoveries led to the development of a new technology for measuring and calculating the IR spectrum used in FT-IR spectrometers, which has dramatically improved the quality of infrared spectra and minimized the time required to obtain data [40].

Thanks to developments in computer technology and substantial price decreases, today there is a large number of commercial FT-IR spectrometers on the market that are used for application of FT-IR spectroscopy in all branches of science and technology.

2.2   Infrared Radiation

First of all, a brief introduction to wave theory is needed. Energies of the electromagnetic spectrum can be considered to be waves that move at the speed of light c, with each type of radiation differing in frequency ν and wavelength λ. The wavelength of the radiation is inversely proportional to frequency. The energy of electromagnetic radiation is, according to Planck's law ($E = h\nu$), directly proportional to frequency, and inversely proportional to wavelength. Therefore electromagnetic radiation can be also characterized by a quantity directly proportional to energy, the so-called wavenumber $\tilde{\nu}$, which is widely used in infrared spectroscopy. This quantity measures the number of waves per unit length and is given by the following relationship: $\tilde{\nu} = 1/\lambda = \nu/c$. The wavenumber[1] is usually expressed in units called reciprocal/inverse centimeters abbreviated as cm^{-1}, but it could be expressed in any reciprocal distance units [40].

---

[1]Energy unit conversion of $1\,cm^{-1} = 10\,mm \cong 30\,GHz \cong 0{,}12\,meV$.)

As already mentioned, spectroscopy studies the interaction of electromagnetic radiation with matter. The interaction is characterized by the energy of the radiation and its effects on materials. In order of increasing wavelength and decreasing frequency and energy, the electromagnetic spectrum consist of gamma rays, X-rays, ultraviolet radiation, visible radiation, infrared radiation, microwaves, radio waves (see Figure 2.1).
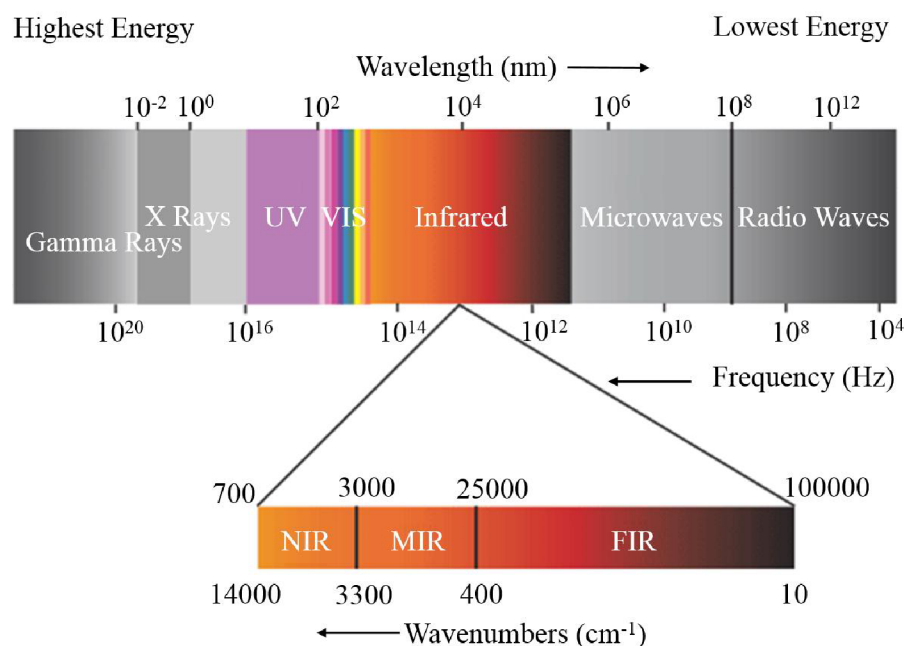
Figure 2.1: The electromagnetic spectrum with highlighted IR region. Adapted from [45].

As was seen in Figure 2.1, the IR spectral region of the electromagnetic spectrum extends from the red end of the visible spectrum to the microwave region; it includes radiation with wavelengths from 700 nm (430 THz) to 1 mm (300 GHz) or wavenumbers ranging from about 14000 to 10 cm^{-1} [43]. Energy of IR radiation is sufficient to produce translational, rotational, and vibrational motion in molecules. Because of application and instrumentation reasons, it is convenient to divide the IR region into three regions: the near (NIR), middle (MIR), and far (FIR) infrared subregions. Many infrared applications employ the MIR region, but the NIR and FIR regions also provide important information about certain materials.

The FIR subregion, lying adjacent to the microwave region, is defined as the region between 25 – 1000 μm (400 – 10 cm^{-1}) [44]. This subregion provides information regarding the vibrations of molecules containing heavy atoms, molecular skeleton vibrations, molecular torsions and crystal lattice vibrations [42].

2.3   Infrared Spectroscopy

The principle of IR spectrocopy is following: a molecule irradiated with infrared radiation absorbs this radiation under some conditions. The energy $h\nu$ of the absorbed radiation is equal to the energy difference between two energy levels of vibration of the molecule (one having an energy E_n and another E_m), which can be written in the form of an equation: $h\nu = E_n - E_m$. In other words, absorption of infrared radiation occurs principally due to a transition between energy levels of molecular vibration, therefore an infrared absorption spectrum is a vibrational spectrum of a molecule. Since molecular vibrations reflect chemical features of a molecule, such as an arrangement of nuclei and chemical bonds within the molecule, IR spectroscopy contributes remarkably not only to identification of the molecule but also to study of the molecule structure. Furthermore, it is useful also in studying the interaction with a surrounding environment which also causes a change in molecule vibrations [41].

2.4   FT-IR Spectroscopy

Fourier Transform Infrared (FT-IR) spectroscopy or in other words, IR Spectroscopy performed on the FT-IR spectrometer is based on the idea of interference of the radiation between two beams to obtain an interferogram[2] shown in Figure 2.2. The second signal is a signal created as a function of the change of pathlength between two beams. The two domains of distance and frequency are mutually convertible by the mathematical method called Fourier transformation [42].

2.4.1   Fourier Transformation

The crucial equations for a Fourier transformation in spectroscopy referring to the intensity incident on the detector, $I(\delta)$, to the spectral power density at a particular wavenumber, $\tilde{\nu}$, given by $B(\tilde{\nu})$, are as follows:

$$I(\delta) = \int_0^\infty B(\tilde{\nu}) cos(2\pi\tilde{\nu}\delta) d\tilde{\nu}, \tag{2.1}$$

which is one half of a cosine Fourier-transform pair and the other is:

$$B(\tilde{\nu}) = \int_{-\infty}^\infty I(\delta) cos(2\pi\tilde{\nu}\delta) d\delta. \tag{2.2}$$

These two interconvertible equations are known as a Fourier-transform pair. The first shows the change in power density as a function of the difference in pathlength,

---

[2]The interferogram is an analogue signal at the detector that has to be digitized in order that the Fourier-transformation into a conventional spectrum can be carried out [42].

which is an interference pattern. The second shows the change in the intensity as a function of wavenumber. Each of them can be converted into the other by the mathematical method of Fourier transformation. The fundamental experiment to obtain an FT-IR spectrum is to create an interferogram with and without a sample in the beam and transforming the interferograms into spectra of (a) the source with sample absorptions and (b) the source without sample absorptions. The ratio of the first and the second corresponds to a double-beam dispersive spectrum. The major progress toward routine used in the mid-infrared region came with a new mathematical method (or algorithm) devised for Fast Fourier Transformation (FFT). This was associated with advances in computers that made it possible for these calculations to be carried out quickly [42].
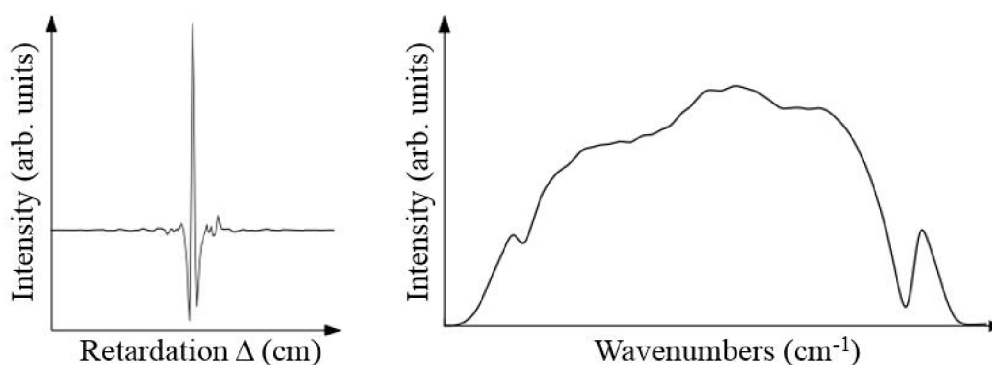
Figure 2.2: Applying Fourier-transform on typical interferogram (left) retrieved from Michelson interferometer allows to calculate the wavenumber spectra (right). Adapted from [46].

2.5 FT-IR Spectrometer

The essential components of the FT-IR spectrometer are schematically shown in Figure 2.3. FT-IR spectrometer primarily includes Michelson interferometer, source of radiation, the detector and other optical elements (beamsplitters, mirrors, etc.). In addition, data manipulation takes place in the adjacent computer station. The radiation originating from the source passes through the interferometer on the sample before reaching the detector. Upon amplification of the signal, in which filters eliminate high-frequency contributions, the data are converted to digital by an analog-to-digital converter and transferred to the computer for Fourier transformation (see subsection 2.4.1). In following text, a brief overview of basic components of FT-IR spectrometer will be described.

| Source | Interferometer | Sample | Detector | Amplifier | Analog-to-digital converter | Computer |
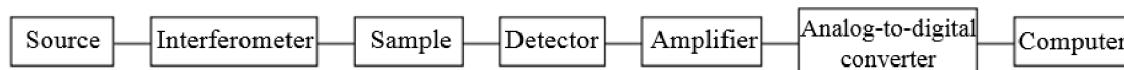
Figure 2.3: The essential components of the FT-IR spectrometer. Adapted from [42].

2.5.1 Michelson Interferometer

The design of the most common interferometers used for infrared spectroscopy today is based on the two-beam interferometer originally designed by Michelson in 1891 [47]. The Michelson interferometer is a device that divides a beam of radiation into two paths and then recombines them after a path difference has been introduced. Because of this path difference, interference can occur between the beams. The variation of intensity of the beam emerging from the interferometer is measured as a function of path difference by a detector. The simplest form of the Michelson interferometer is shown in Figure 2.4 [44].

Fixed Mirror

Source

Movable Mirror

Movement

Beamsplitter

Detector
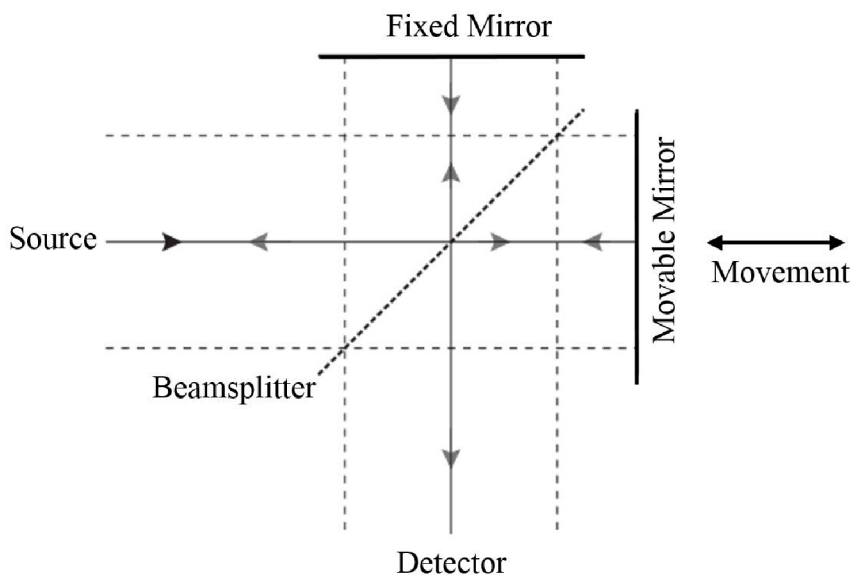
Figure 2.4: Michelson interferometer. Adapted from [44].

The Michelson interferometer consists of two mutually perpendicular planar mirrors, one of which can be moved along an axis which is perpendicular to its plane. A beamsplitter bisects the planes of these two mirrors. A collimated beam of monochromatic radiation of wavelength λ from the source is partially reflected to the fixed mirror and partially transmitted to the movable mirror. In the case of the ideal beamsplitter, 50% of the incident radiation is reflected while 50% is transmitted. The two beams reflected from these mirrors then return back to the

beamsplitter where they recombine and interfere and they are again partially reflected and partially transmitted. For the ideal case, 50% of the beam reflected from the fixed mirror is transmitted through the beamsplitter while 50% is reflected back in the direction of the source. The beam emerging from the interferometer at 90° to the input beam is called the transmitted beam and this is the beam detected in FT-IR spectroscopy. The moving mirror produces an optical path difference between the two arms of the interferometer. For path differences of $(n + 1/2)\lambda$, where n is the order of interference pattern, λ is the wavelength of incident radiation, the two beams interfere destructively in the case of the transmitted beam and constructively in the case of the reflected beam. For path difference of $n\lambda$, the two beams interfere constructively for the transmitted beam, and destructively for the reflected beam [42, 44].

2.5.2 Sources

FT-IR spectrometers use a Globar or Nernst source for the MIR region. Globar source is made out of silicon carbide (SiC) and it has metallic leads at the ends which serve as electrodes. The use of electric current leads to the generation of heat, which yields radiation at temperatures higher than 1000 °C. The electrodes need to be cooled, therefore water cooling is required for this type of source. The spectral energy density of blackbody sources is always below $200\,\text{cm}^{-1}$ and the problem of measuring far-infrared spectra is associated with the fact that the emissivity of Globars and Nernst sources is much less than that of the far infrared. For the near-infrared, tungsten–halogen lamps are used [41, 44]. Measurements of FIR spectra are made far more difficult than the corresponding measurement of MIR or NIR spectra due to the weakness of the source. Since the sensitivity of any measurement of a MIR or FIR spectrum is directly proportional to the spectral energy density of the source, the FIR sources should be as hot as possible and have high emittance. Therefore, if the FIR region is to be examined, then the standard source that is used for FIR spectroscopy is a high-pressure mercury lamp (mercury arc or Hg-Arc lamp). The reason why mercury lamps are so popular for FIR spectroscopy is because emission from the plasma intensifies the emission from the hot quartz envelope of the lamp. However, this kind of lamp has significant flicker noise, so even if the energy is better, the signal-to-noise ratio may not be [44, 48].

2.5.3 Detectors

One of the most important components of an infrared spectrometer is the element responsible for the detection of infrared energy. There are two classes of infrared detec-

tors. One class comprises the thermal detectors which operate by sensing fluctuations in the temperature of an absorbing material as a result of exposure to the incoming radiation. The other class are the photon detectors (also called quantum detectors) which are sensitive to changes in the quantity of free-charged carriers in the solid, brought by the interaction with the external radiation. In IR spectroscopy, the detector noise (the fluctuation in signal intensity for a steady radiation field) is usually much higher than any other noise source and it has usually a thermal origin [41]. Therefore, IR detectors usually do not operate at room temperature. The normal detector for routine use is a pyroelectric device incorporating deuterium triglycine sulfate (DTGS) from the group of thermal detectors. For more sensitive work, mercury cadmium telluride (MCT) cooled to liquid nitrogen temperatures is used [41, 42]. In the FIR region, boron-doped silicon or germanium doped with copper, gallium or antimony detectors are employed which operate at liquid helium temperatures [44].

2.5.4 Parabolic Mirrors

In commonly used FT-IR spectrometers, the radiation emitted by the source is collected and collimated, passed through the interferometer, brought to a focus in the sample compartment and refocused onto the detector. The beam from the source is usually collimated with an off-axis parabolic mirror before it passes through the interferometer. This type of mirror is needed because any line parallel to the axis of a parabola is reflected through its focus (see Figure 2.5). Rotation of the parabola about its axis creates a paraboloid. Thus, any collimated beam of radiation parallel to the axis of a paraboloid is reflected through its focus [44].
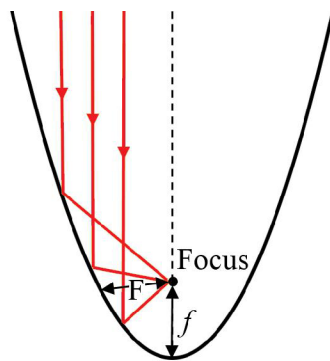

Figure 2.5: Typical parabola, with focal length f. For the off-axis section shown on this figure, the effective focal length is F.

2.6 Spectral Analysis

The output from the spectroscopic instrument is referred to as a spectrum. An infrared spectrum is commonly obtained by passing infrared radiation through a sample. Some of the incident radiation is absorbed by the sample and some of it passes through (transmitted radiation). The resulting spectrum represents the molecular absorption and transmission creating a typical molecular fingerprint of the sample. Early infrared devices recorded percentage transmittance over a linear wavelength range. Nowadays, it is unusual to use wavelength for routine samples and the wavenumber scale is used instead [42].

2.6.1 The Beer-Lambert Law

The Beer–Lambert law can be used to relate the amount of light transmitted by a sample to the thickness of the sample. The absorbance of a solution is directly proportional to the thickness and the concentration of the sample, as follows: $A = \epsilon c l$, where A is the absorbance of the solution, c is the concentration, and l is the pathlength of the sample [42]. The constant of proportionality ϵ, is referred to the molar absorptivity. The absorbance is equal to the difference between the logarithms of the intensity of the light entering the sample (I_0) and the intensity of the light transmitted (I) by the sample:

$$A = log I_0 - log I = log(I_0/I). \tag{2.3}$$

Absorbance is therefore dimensionless. Transmittance is defined as follows:

$$T = I/I_0, \tag{2.4}$$

and percentage transmittance as: $\%T = 100 \times T$. Thus:

$$A = -log(I/I_0) = -log T. \tag{2.5}$$

By using percentage transmittance values, it is easy to relate and to understand the numbers. For example, 50% transmittance means that half of the light is transmitted and half is absorbed, while 75% transmittance means that three quarters of the light is transmitted and one quarter absorbed [42].

2.6.2 Signal and Noise

Since the intensity of radiation in spectroscopic experiments is usually very low, noise and statistical errors play an important role. The quantity which that characterizes this problem is called signal-to-noise ratio. Radiation detection is determined by its

quantum nature. The photon is either absorbed or not in a process relevant to the detection scheme. For a better description by probability theory, signal can be called as the number of events k of photon absorption processes out of a number of $n \geq k$ incident photons. Each absorption process has a probability p and the probability that no absorption occurs or that absorption does not contribute to the signal is $q = 1 - p$. This approach is valid for many radiation detectors. The probability for the constructive absorption of k photons is given by the binomial distribution. For small values of p, it can be well approximated by the Poisson distribution

$$P(k, n) = \frac{y^k}{k!} e^{-y}, y = np \approx \langle k \rangle. \tag{2.6}$$

For n large, y is the mean value $\langle k \rangle$ of the distribution or the average magnitude of the signal. Since P is a probability, also other values of k may be observed. This means that the mean signal $\langle k \rangle$ is accompanied with noise. The square root of the variance σ^2 of the distribution P can be definition for the noise. Calculation yields $\langle k \rangle$ for the variance of the Poisson distribution, so the variance is equal to the mean value. Then, the noise is

$$\sigma = \sqrt{\langle (k - \langle k \rangle)^2 \rangle} = \sqrt{\langle k^2 \rangle - \langle k \rangle^2} = \sqrt{\langle k \rangle}. \tag{2.7}$$

Signal $\langle k \rangle$ increases linearly with the length of the measuring time T, so the noise increases as the square root of T. Therefore, the signal-to-noise ratio, the important quantity defining the accuracy of the measurement, increases as $\sqrt{T}$ [49].

2.7 Far-Infrared Spectroscopy in High Magnetic Field

High magnetic field has become an important research tool for studying the characteristics of materials in many scientific disciplines. In general, spectroscopy can be defined as observation of transitions between energy levels of materials, where the spectrum is a display of the dependence of some property of a sample as a function of some other parameter, for example, energy absorption *versus* energy. The use of high magnetic fields in combination with optical spectroscopy, such as FIR spectroscopy, has the potential of making great contributions to science and technology. In addition, magneto-optical experiments provide a powerful set of tools to obtain insights into the properties of materials. Such experiments are often an ideal way to study new physical phenomena, because many physical phenomena depend explicitly on the presence of a high magnetic field. FIR energy region in high magnetic fields is of particular importance, since it covers the magnetic resonances

such as spin resonance, cyclotron resonance and other important effects. FIR radiation is also important because its low energies (meV range) are such that electronic and magnetic states are probed very near their equilibrium state (measuring essentially ground state properties) [50].

In summary, FIR Spectroscopy in high magnetic fields presents an ideal experimental technique that can probe and elucidate properties of advanced materials such as graphene [51]. Furthermore, this technique provides complementary information to the more commonly used measurements of transport, magnetization, and thermodynamic properties [50].

The following text thus presents some scientific institutes and laboratories around the world that have magneto-optical setup which combines IR spectroscopy and high magnetic fields.

- **Basov Infrared Laboratory – San Diego, CA, USA**
  (University of California, San Diego — Department of Physics)
  The system, shown in Figure 2.6, is capable of broadband frequency domain spectroscopy in the range 180 GHz to 750 THz at cryogenic temperatures. The reflection unit couples both the Martin-Puplett and the Michelson interferometer to a 9 T superconducting split coil magnet. Additionaly the unit is designed to work with various detectors, including thermal bolometers and semiconducting detectors [52].
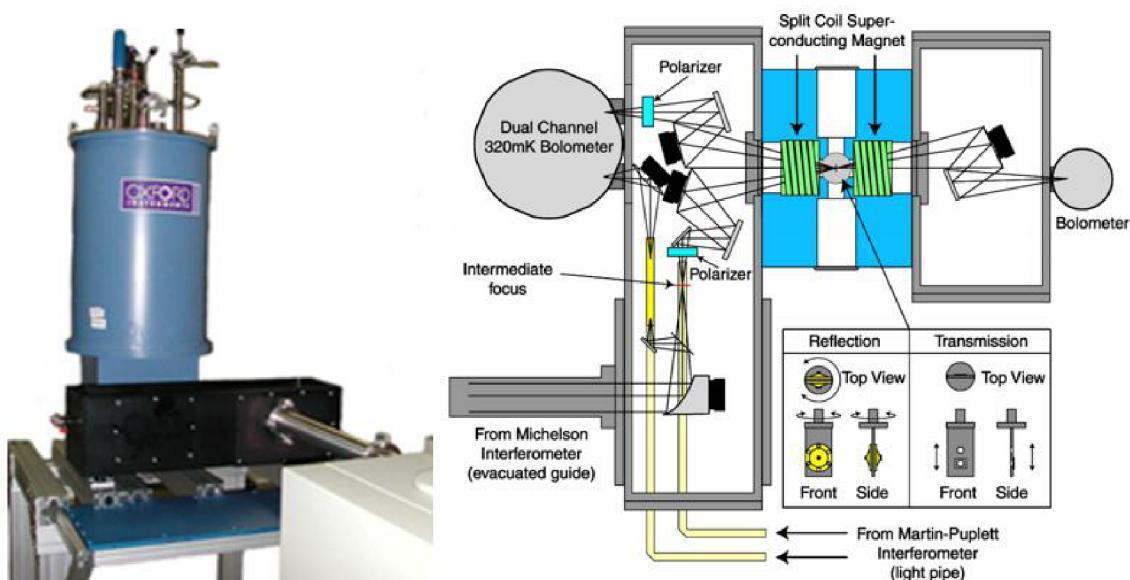
Figure 2.6: Basov Infrared Laboratory in San Diego at University of California, USA with scheme of the optical layout of their apparatus [52, 53].

- **IR-spectroscopy laboratory – Zurich, Switzerland**

  (ETH Zürich, Department of Physics – Laboratory for Solid State Physics)

  The IR spectroscopy laboratory (shown in Figure 2.7) is equipped with a FT-IR spectrometer combined with an Oxford cryostat (SM4000). This facility allows to perform IR optical investigations from 300 down to 1.8 K in external magnetic fields from 0 T up to 8 T. A specially designed optics by Bruker extracts the IR beam from Vertex 80v allowing measurements in reflection mode. The cryostat is equipped with suitable optical windows, which permit measurements from FIR up to the MIR spectral range [54].

Figure 2.7: IR spectroscopy laboratory in Zurich, Department of Physics – Laboratory for Solid State Physics [54].

- **Visible and IR magneto-optical system – Warsaw, Poland**

  (University of Warsaw, Institute of Experimental Physics – Division of Solid State Physics)

  Oxford Instruments Spectromag 4000-8 cryostat has four strain-free windows and enables a variety of magneto-optical experiments (transmission, reflectance, photoluminescence, Faraday and Kerr effects, etc.) in magnetic fields up to 8 T and temperatures down to 1.3 K [56].

- **Magneto-optical THz laboratory in Geneva, Switzerland**
  (University of Geneva)
  The magneto-optical THz laboratory shown in Figure 2.8 utilize FT-IR or time-domain THz spectroscopy with magnetic field up to 7 T (superconducting coil) in transmission, reflection, Faraday rotation or Kerr rotation mode measurements [55].

Figure 2.8: Magneto-optical THz laboratory at University of Geneva in Switzerland [55].

- **The High Field Magnet Laboratory at Radboud, the Netherlands**
  (University Nijmegen)
  The far infrared (FIR) spectroscopy using both fixed frequency/swept field and broad-band frequency domain with fixed field. Currently, only the transmission measurement in the Faraday configuration is available; Voight configuration and reflectivity are under development. The signal is detected using a sample probe which contains a He cooled Si bolometer. There are two modes of experimentation: Fixed frequency, sweeping field, using an optically pumped

molecular laser. The radiation is guided to the sample using an oversized waveguide. Fixed field, broad-band ($12-700$ cm^{-1}) spectroscopy uses a Bruker IFS 113v FT-IR spectrometer with a Hg-Arc lamp, a quasi-optical telescope is used to transport the radiation down to the sample tube, where it is guided through the sample and onto the detector [57].

- **Grenoble High Magnetic Field Laboratory (GHMFL), France**
  (French National Center for Scientific Research (CNRS))
  The setup at GHMFL consists of Bruker IFS 66v/s FT-IR spectrometer with a Hg-Arc lamp source, where the sample is placed inside the 11 T solenoid magnet, with a composite bolometer detector element located inside the magnet.

3 Design of the Magneto-Optical Setup

In this chapter, reasons for the development of the FIR spectroscopy in high magnetic field will be clarified and the design of the magneto-optical setups will be described in detail.

The motivation for the design and the development of the setups which utilize the FIR spectroscopy in a high magnetic field is that such a combination presents a very important tool in the characterization of SMMs, SIMs [58] and other materials such as graphene [51]. For example, the setup that combines the FT-IR spectrometer and the superconductive magnet allows studying magnetic resonance phenomena such as EPR through the use of the FIR spectroscopy. This technique can probe and elucidate properties of SMMs with very large zero-field splitting, mainly based on transition metal complexes [16] or lanthanides [6], in which commonly used EPR systems do not provide experimental access to the magnetic resonance transitions.

Main inspiration for this thesis – coupling of a FT-IR spectrometer to a superconductive magnet at CEITEC – was the setup, which has been designed during my six-month internship in Germany at University of Stuttgart, Faculty of Chemistry, Institute of Physical Chemistry (IPC) in the group of Prof. Joris van Slageren under the supervision of Dr. Petr Neugebauer. This research group focuses mainly on the investigation of SMMs which can be used for future data storage or quantum computing, by means of advanced spectroscopic methods such as EPR spectroscopy and other. In order to provide EPR spectra of SMMs in FIR region and to perform first magneto-optical experiments in FIR region at IPC, I was given the task to design the coupling of the FT-IR Spectrometer Bruker VERTEX 70v to a 15/17 Tesla superconductive magnet. As a result of the coupling, a magneto-optical setup was built up at IPC in Stuttgart. The setup is already assembled and put into the operation. Its performance is discussed in the experimental part (Chapter 4). Additionally, magneto-optical measurements of SMM performed on this setup are presented in chapter 4. The setup at IPC in Stuttgart was essentially a "springboard" for my master's thesis. The second described magneto-optical setup is designed for CEITEC. Its design draws on the experiences gained in the first setup. In following, a detailed description of both magneto-optical setups will be provided.

3.1 Magneto-Optical Setup at IPC

The first magneto-optical setup described in this thesis is the setup designed for IPC of the University of Stuttgart. Schematic figure of the magneto-optical setup in Stuttgart, where all its components are labeled, is shown in Figure 3.1. This setup consists of Oxford Instruments 15/17 T solenoid cryomagnet, used primarily for HF-EPR configuration (see subsection 1.2.2), FT-IR Spectrometer Bruker VERTEX 70v equipped with an FIR source (external water cooled mercury Hg-Arc lamp), a detector – pumped liquid helium bolometer (Infrared Laboratories HDL-5) – and then the components coupling the spectrometer to the magnet, which were designed during my internship: movable table, optical system and transmission probe. These components were designed in the 3D design CAD[1] software Inventor from Autodesk. Then they were manufactured at the IPC workshop. The emphasis was to ensure that all components manufactured for the magneto-optical setup were and made from non-magnetic materials, i.e. brass, aluminum, nickel silver or non-magnetic stainless steel, to avoid possible complications from strong forces caused by stray fields of the superconductive magnet. Another criterion for material choice was the suitability for cryogenic temperatures. In the following text, all these components will be sequentially described in more detail.

3.1.1 Movable Table

In the beginning, the task was to design a compact movable table on which spectrometer would be laid with all its equipment and accessories. The reason for that was that the spectrometer is shared with another department which uses it for classical Infrared Spectroscopy measurements in their laboratory. In order to enable easier transfer of the spectrometer between the laboratories, this table had to be movable. Figure 3.2 (a) shows a 3D model of the folded and unfolded movable table together with its final version with the spectrometer and its accessories in (b).

The table (shown in Figure 3.2) was equipped with four rubber wheels to reduce vibrations during transportation, four leveling feet to secure final position in the laboratory during measurement, two shelves for all equipment including computer, removable board for bolometer, handle for better manipulation during transport, folding board for possible table extension. For better access to the magnet, a cut out was made in the bottom shelf. Table size was adapted to fit in the elevator and pass the doors. The frame of the movable table was made of KANYA aluminium profiles (40 mm) and all boards were made of wooden boards.

---

[1]Computer-Aided Design
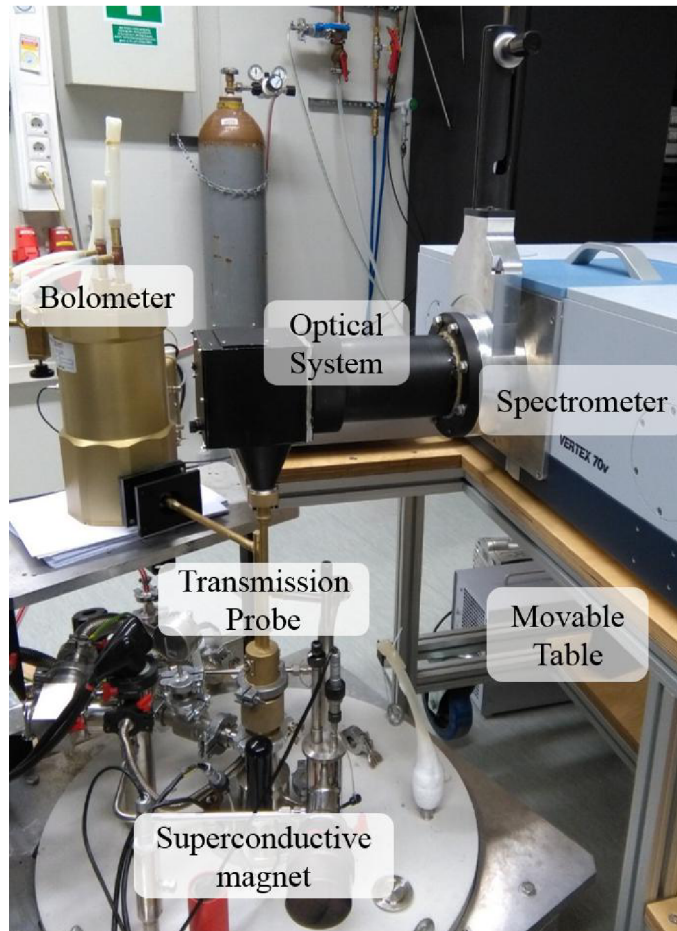
Figure 3.1: The magneto-optical setup at Institute of Physical Chemistry (IPC), University of Stuttgart. It consists of the Oxford Instruments 15/17 Tesla solenoid superconductive magnet, the Bruker VERTEX 70v FT-IR spectrometer, the Infrared Laboratories liquid helium bolometer and components designed during the internship: the movable table, the optical system and the transmission probe.

3.1.2 Optical System

The second task was to design a part – optical system – which would couple the spectrometer with the superconductive magnet. In Figure 3.3, a final look of the optical system is depicted (a) together with a 3D model (b) and its cross-section (c), where all mentioned components are labeled and a direction of the beam is shown.

The optical system (Figure 3.3) has been designed for guiding the beam from the spectrometer to the transmission probe placed inside of the superconductive magnet. The magnet has been incorporated in the beam path between the spectrometer and the detector of the radiation. For guiding the beam out of the spectrometer, the

Figure 3.2: (a) 3D model of the folded and unfolded movable table with a scale, (b) final look of the movable table with the spectrometer and its accessories (Infrared Laboratories bolometer).

Reflection Unit A515 for External Focus from Bruker (Figure 3.4), belonging to accessories of the spectrometer, was used. This unit was integrated to the sample compartment of the spectrometer. It consists of the symmetrical system of mirrors. Only half of them is used to focus the beam from the source and then guide it out of the spectrometer. Disadvantage of this unit is, that it guides out a focused beam instead of a parallel beam. Parallel beam is convenient for a parabolic mirror, because any incoming rays parallel to its axis are reflected to a focus point (see 2.5.4).

For the purpose of guiding the beam out of the spectrometer, the original door plate in the front the spectrometer was replaced by a new one, in which an opening with the diameter of 100 mm was formed. In order to separate the spectrometer from the optical system, vacuum gate valve from company VAT with the inner diameter of 100 mm and manual actuator (push rod) was installed onto the door plate. When it is desired to use only the spectrometer without the optical system, this valve can be easily closed.

For guiding the beam further into the optical system (Figure 3.3), a guiding tube with the inner diameter of 100 mm was pressed by an interference fit to a flange, which was mounted to the gate valve. On the opposite side of this tube, pins were placed to secure the proper position of the housing, in which the parabolic mirror was situated. The housing and the guiding tube are connected together by a ring with inner thread, which is put on the guiding tube, and a thread mounted into the front plate of the housing. In the housing, Thorlabs $\varnothing 3$" $90°$ Off-Axis Parabolic
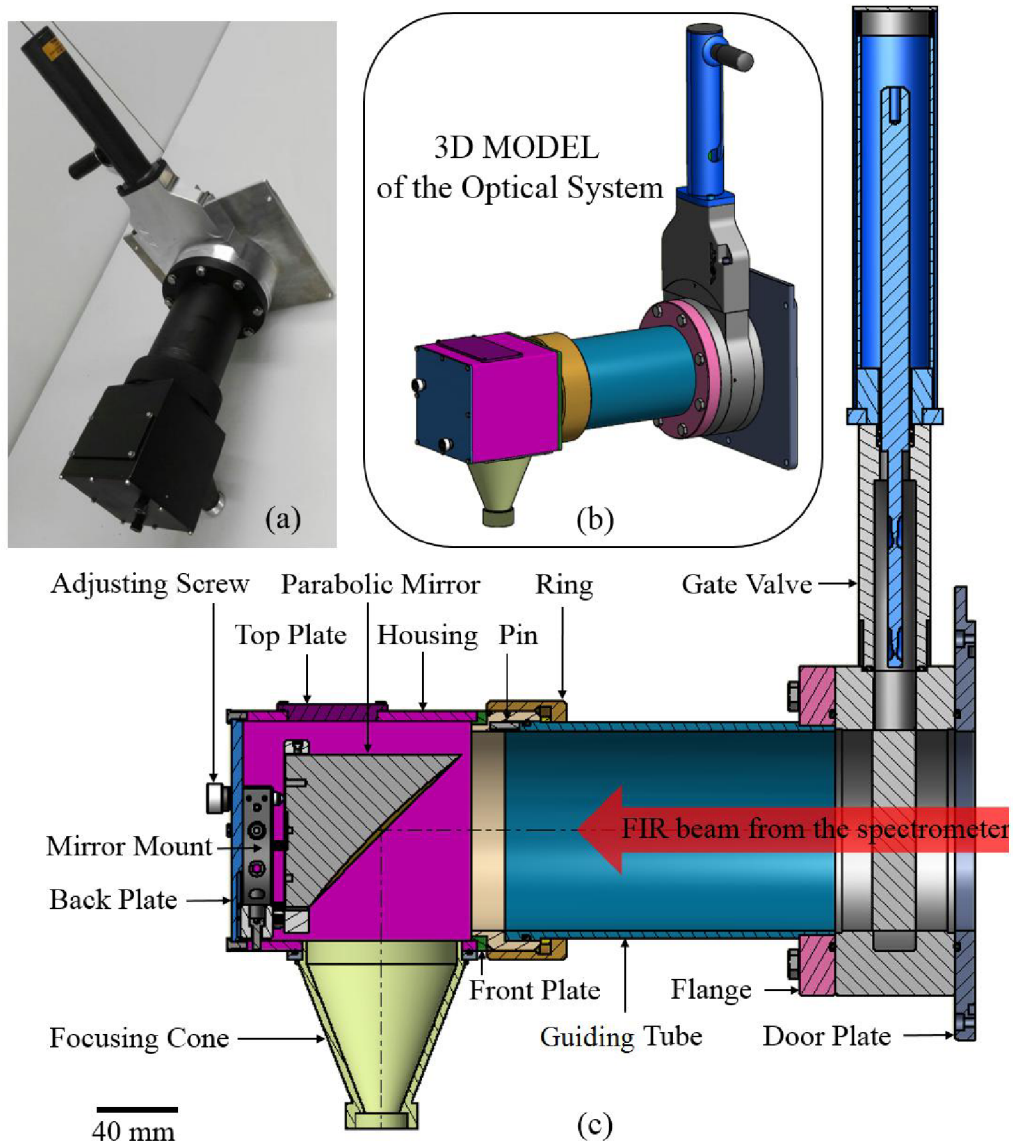
Figure 3.3: Schematic figure of the optical system: (a) a final look of the optical system (aluminium components are coated with a black dye layer by anodizing) (b) a miniature 3D model of the optical system (in a frame) and (c) its cross-section with a scale where all mentioned components are labeled and a direction of the beam is shown.

Mirror ($RFL^2 = 152.4\,\text{mm}$) with gold coating[3] was implemented to reflect the beam and rotate it by 90°. It was inserted in the Thorlabs Mirror Mount, which was installed in the housing by two screws. On the back plate of the housing, two sealing openings were made for two adjusting screws, which are used for the alignment of

---

[2]Reflected Focal Length

[3]Gold coating offers a broad and consistent reflectivity in the FIR range [59].

Figure 3.4: The Reflection Unit A515 for External Focus from Bruker which consists of the symmetrical system of mirrors. Half of them is used to focus the beam from the source and then send it focused out through an opening in the spectrometer.

the parabolic mirror. An opening for eventual manipulation with the mirror was created on the top of the housing. It was covered by a removable top plate that was mounted to the housing. To secure a smooth transition of the beam reflected from the parabolic mirror to the transmission probe, the focusing cone was used. An opening for this cone was formed on the bottom side of the housing, in which the focusing cone was inserted and installed. The end of the focusing cone was finished by a thread on which is then mounted the transmission probe (see subsection 3.1.3).

During the sample exchange, the housing with the parabolic mirror and the focusing cone is taken off by using the ring mounted on the guiding tube, whereas the guiding tube with the gate valve is still connected to the spectrometer.

In order to reduce radiation losses, the spectrometer together with the optical system is pumped out to prevent atmospheric absorption. Components are thus equipped with o-rings at every joint of two parts. All designed components of the optical system were made of aluminium. These components, with exception of the gate valve and door plate, were covered with a black coating layer by anodizing[4] in order to avoid creating of reflections and scattering of the beam.

3.1.3   Transmission Probe

For the design of this probe, an old unused transmission probe from the microwave HF-EPR configuration was modified. Only the upper part of this probe was newly

---

[4]Anodizing, an elox or anodic oxidation, is an electrolytic passivation process that is used to form a protective oxide layer on the surface of aluminum components to increase corrosion resistance and to allow dyeing.

designed. Figure 3.5 shows a cross-section of the whole probe with labeled components and beam propagation, a 3D model of the upper part of the transmission probe (in a frame) which was newly designed (b), and a final look of the top of the probe (c).

Figure 3.5: Schematic figure of the transmission probe: (a) a cross-section of the whole probe with a scale where all mentioned components are labeled and a propagation of the beam (red) is shown, (b) a miniature 3D model of the upper part of the transmission probe (in a frame) which was newly designed and (c) a final look of the top of the probe with the Mylar window.
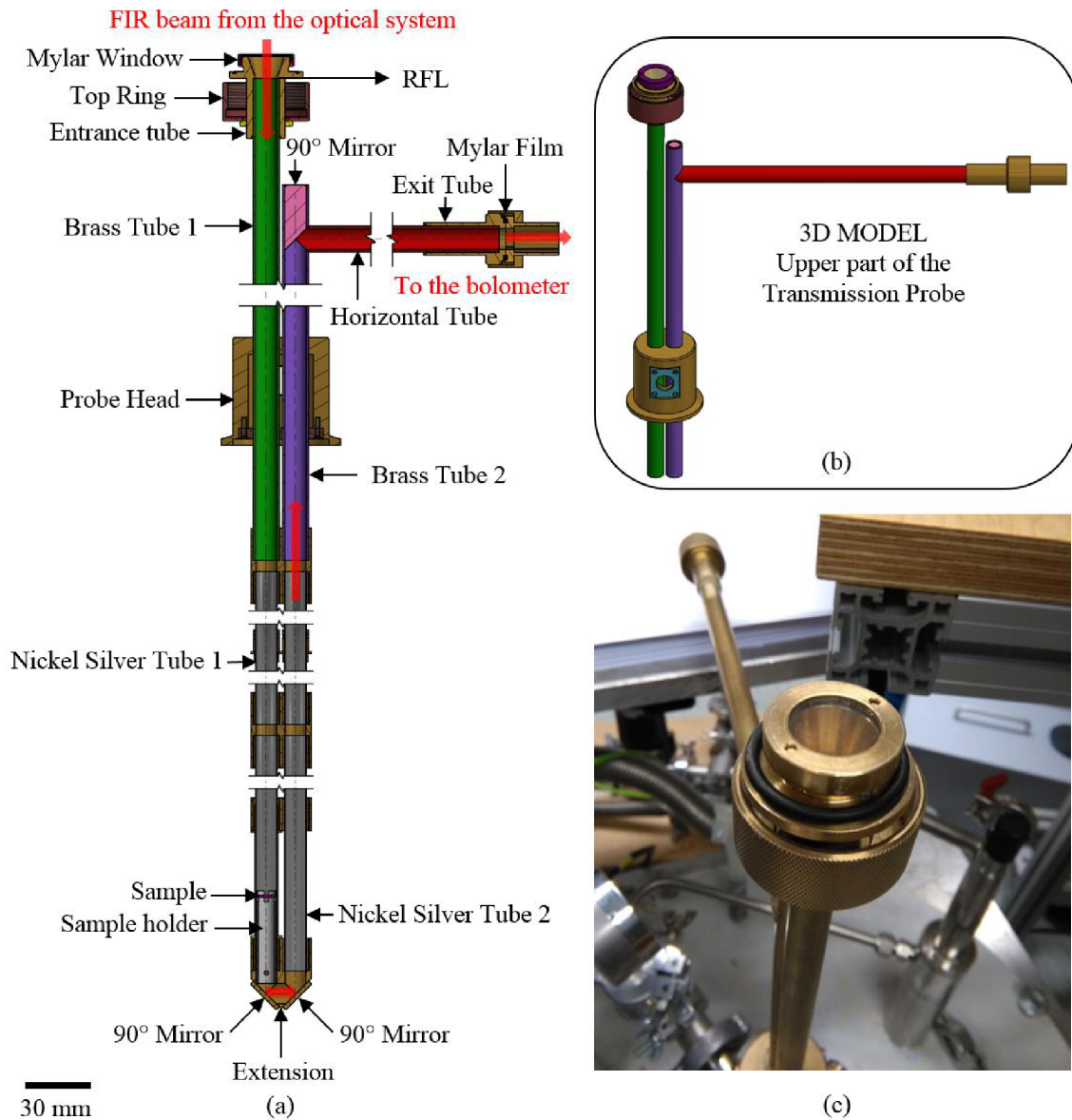
The upper part of the transmission probe (Figure 3.5) contains three brass tubes

with the inner diameter of 10 mm. The brass tube 1 has the entrance tube with the inner threaded top ring mounted on its top for connecting the probe with the optical system. The top ring is installed directly onto the focusing cone of the optical system (see subsection 3.1.2). On the top of the entrance tube, a window with a 16 μm thick Mylar[5] film is mounted. The optical system is up to this Mylar window placed under the rough vacuum by the pump of the spectrometer. In order to separate the probe from the evacuated optical system, the mylar window is used because the probe is after inserting to the VTI of the magnet filled with cryogenic helium gas.

The brass tube 1 and 2 are embed to the probe head. The probe head is after inserting of the probe into the VTI, attached to the magnet by DN50 KF flange. At the end of these tubes, the original part of the probe which has two nickel silver tubes with the inner diameter of 10 mm, was mounted.

The beam propagating from the optical system passes through the Mylar window and enters the brass tube 1 (Figure 3.5). The focal point of the parabolic mirror is designed to be right at the input to the brass tube 1 to reduce losses. The focused beam in the brass tube 1 is guided to the nickel silver tube 1 with the sample holder at the bottom. The sample holder is designed pressed powder pellet samples with the diameter of 8 mm. When the beam reaches the sample placed in the sample holder, which is Faraday geometry[6], it is transmitted and continues further till it reaches the extension. The extension connects both ends of the nickel silver tubes and it has two small mirrors rotated by 90° installed at the bottom. These mirrors reflect and guide the transmitted beam from the nickel silver tube 1 through the extension to the nickel silver tube 2. Then it propagates to the brass tube 2, where another 90° mirror is located. The beam is from this mirror reflected and propagates through the horizontal brass tube 3 through another Mylar film placed in the exit tube, which was installed at the end of this tube. This window separates the probe from outside because the probe from the evacuated optical system, the mylar window is used because the probe is after inserting to the VTI of the magnet filled with cryogenic helium gas. By passing through this window, the beam is going straight to the bolometer.

During my internship in Stuttgart, I have designed also another, a brand new, probe for a configuration with the detector placed inside of the cryostat, under the sample. This probe can be used not only for FIR configuration, but it can be easily adapted for the microwave quasi-optics configuration. However, the description of this probe will not be provided here because it is out of the scope of this thesis.

---

[5]the commercial name for polyethylene terephthalate

[6]Faraday geometry: incident light is propagating parallel to the applied magnetic field and the magnetic field is always oriented perpendicular to the sample.

3.1.4 Proposed Improvements

This part propose improvements for the magneto-optical setup at IPC in Stuttgart. Main problems are described, and the solutions to these problems are suggested here.

During the assembly of the setup and putting it into the operation, several problems have been discovered and identified. The following paragraphs serve as a "troubleshooting" of the setup which summarizes the main problems that have occurred, suggests their solutions and thus basically proposes improvements of the setup.

- **Vacuum problem:** Some joints between parts of the optical system were not vacuum tight. Parts fabricated by an interference fit, for example, the guiding tube pressed in the flange were leaking. This problem was solved by using a vacuum epoxy which sealed the leaks. To avoid this problem to occur in the future, it is suitable not to use an interference fit at such joint. Another option is to use welding or a copper gasket, which is commonly used in vacuum equipment to mate two Conflat (CF) vacuum flanges together. Other smaller leaks in the system were solved again by using a vacuum epoxy.

- **Reflection unit problem:** The problem of this unit is, as already mentioned, that it sends out a focused beam instead of a parallel beam which is convenient for the parabolic mirror. Therefore, the beam reflected by the parabolic mirror is not so well focused like in the case with a parallel incident beam. Due to this problem, it is possible that a part of the signal is lost. The solution to this problem is not to use this unit and guide the parallel beam out through one of five originally designed output openings in the spectrometer (see Figure 3.8).

- **Bolometer connection problem:** There is a problem that the probe ending 2 of the transmission probe is not properly connected to the window of the bolometer. It is just loosely attached to this window. Therefore, there is a small air gap (the order of millimeters) between the exit tube and the bolometer that can cause atmosphere absorption bands in the spectra during measurements. Another issue, the mutual position of the bolometer and the exit tube is not secured. Therefore, every time when the bolometer or probe is moved, this position changes and it influences the quality of the signal. The solution can be a design of a plate, which will be mounted on the exit tube and this plate will be then installed to the bolometer.

- **Mylar film problem:** The transmission probe has two Mylar film windows which are used for a separation of the probe from the optical system and from the outside. Mylar film is the most commonly used material for IR spectroscopy

windows at cryogenic temperatures. It has sufficient strength to withstand atmospheric pressure for reasonable film thicknesses, and it is not cracking at low temperature. A major disadvantage of Mylar as an IR window material, is the presence of strong absorption lines between 400 and $2000\,cm^{-1}$. The solution to this problem is using other materials as the windows in the probe, for example, polypropylene windows. It was shown that polypropylene film has the necessary strength to serve as a vacuum window from room temperature to superfluid helium temperature and has transmission properties much superior to the commonly used Mylar windows. It has fewer and much weaker absorption bands than Mylar below $2000\,cm^{-1}$and no observable absorption bands below $800\,cm^{-1}$ [60]. Since the windows in the probe are designed to be easily exchanged, this problem can be readily fixed.

- **Sample holder problem:** During the testing of the system and first magneto-optical measurements of samples, it was noticed that a sample is not stably placed in the sample holder and needs to be fixed because it sometimes flips during pumping of the VTI or by inserting the sample holder to the probe (see Figure 3.6 (a)). Therefore, a counterpart to sample holder was additionally designed, which is shown together with sample holder in Figure 3.6 (b), (c).

(a)　　　　　　　　(b)　　　　　　　　(c)
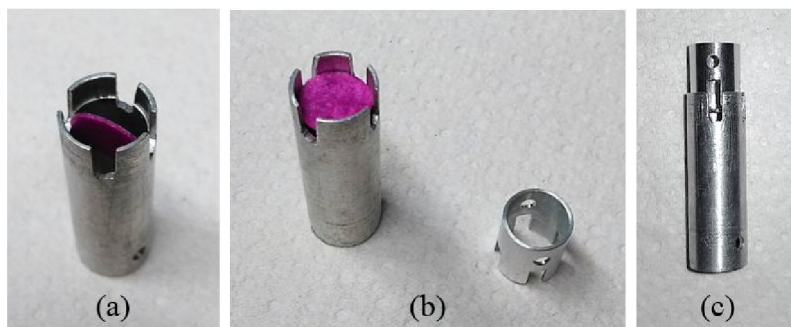
Figure 3.6:　The sample holder problem and its solution: (a) flipped sample in the sample holder, (b) proper position of the sample in the sample holder with newly designed counterpart and (c) the sample holder with its counterpart for fixing a proper position of the sample in the sample holder.

- **Sample/Reference problem:** Another issue of this setup is that the transmission probe is designed only for one sample measurement. There is no possibility to measure sample and reference at the same conditions because there is not enough space in the bore of the magnet for the sample holder with two openings enabling to switch between sample/reference during one measurement. One option for solving this issue is to redesign the probe and create sample

holder for sample and reference, but according to not enough space, it could be complicated. Another option is to use a magnet with a wider bore.

This troubleshooting has formed a good basis and starting point for a new and improved design of the magneto-optical setup which will be built at CEITEC. In the following text is the new design thoroughly described.

3.2 Magneto-Optical Setup at CEITEC

This section has a structure similar to a previous one, but the design of the magneto-optical setup at CEITEC will be described in more details because it is essential for this thesis.

The second magneto-optical setup described in this thesis is basically an improved version of the setup at IPC and it is designed for CEITEC. It consists of Cryogenics Ltd. 16 Tesla cryogen-free superconductive magnet with the 50 mm (diameter) VTI, FT-IR Spectrometer Bruker VERTEX 80v [61] equipped with an FIR source (external water cooled mercury Hg-Arc lamp), the detector – a pumped liquid helium bolometer (Infrared Laboratories HDL-5) – and then the components coupling the spectrometer with the magnet, which were designed for the purpose of this thesis: optical system, transmission probe. These components were again designed in software Inventor from Autodesk. They are made from non-magnetic materials due to the same reason as stated in the first setup. Moreover, mu-metal[7] plate is used to shield sensitive electronic equipment against static or low-frequency magnetic fields in this setup.

Part of this setup is also the movable table, which is modified version of the table which was designed by Ing. Antonín Sojka for the broadband EPR spectrometer based on THz rapid frequency scans (THz-FRaScan-EPR) at CEITEC. Therefore, this table will be mentioned and described only marginally.

In the following text, all these components are sequentially described in more details, and the propagation of the beam is illustrated and clarified there. Because this setup is not yet manufactured at the time of submitting the thesis, in this section will be provided only pictures of 3D models.

3.2.1 Movable Table

The movable table for FIR spectroscopy measurements is created in order to provide easy sample exchange, quick adjustment and precise alignment of the setup. On this table, the spectrometer with all its equipment and accessories will be placed. The

---

[7]nickel–iron soft ferromagnetic alloy with very high permeability [62]

table (shown in Figure 3.7) is modified version of the compact movable table which was designed for the THz-FRaScan-EPR configuration. It is equipped with linear guide rails, four wheels for transfer, drawers, and shelves. It also has a specially designed shelf for the bolometer. Motion is automatically driven by a servomotor and trapezoidal screw. Thanks to the automatically driven motion, the spectrometer with optical system will be precisely aligned to the transmission probe inserted in the superconductive magnet. During the sample exchange, no parts need to be take off, as in the previous setup, only the table will be shifted to pull the probe out from the magnet. For classical IR spectroscopy measurements, the table can be easily taken from the rails, placed on wheels and moved to the desired location.
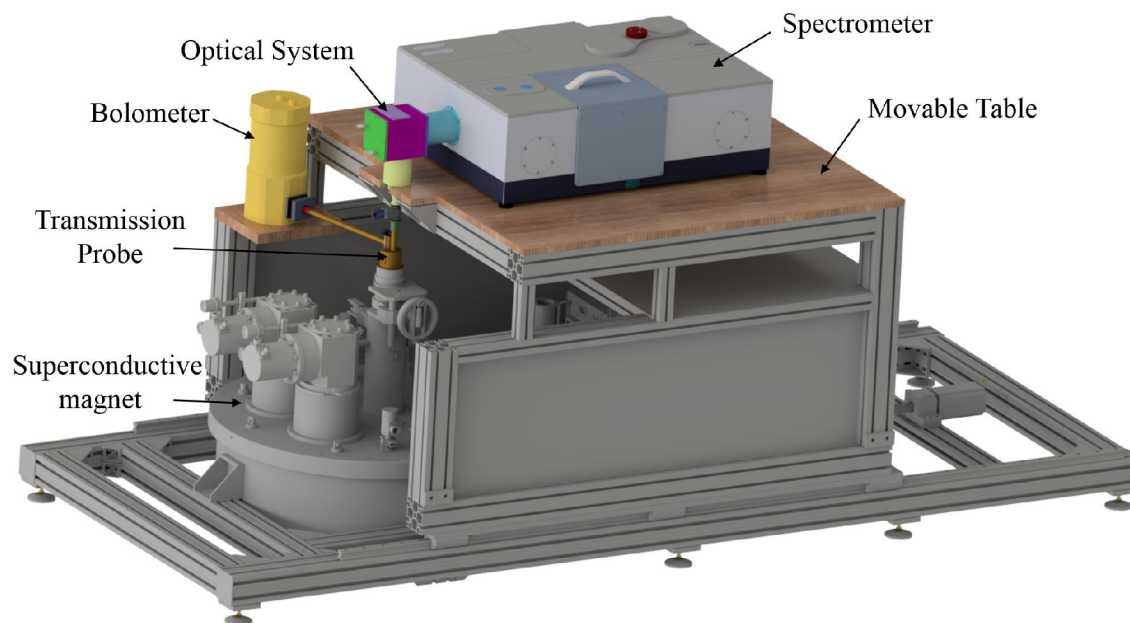
Figure 3.7: 3D model of the compact movable table placed on rails. On the table, the spectrometer with the optical system is placed and attached to the transmission probe which is inserted into the superconductive magnet. The bolometer is placed on the special shelf.

3.2.2   Beam propagation

Unlike the previous setup, for the beam propagation out of the spectrometer the reflection unit is not used, but the beam from the spectrometer is guiding out through one of five originally designed openings/outputs in the spectrometer. The schematic figure of the FT-IR spectrometer Bruker VERTEX 80v with the beam path (red) is shown in Figure 3.8 (a). The output 2 (OUT 2) was chosen for this purpose, because it seemed to be the most advantageous choice. It is simply the shortest and

the easiest path to guide the parallel beam out of the spectrometer and the beam by this path passes through the smallest number of optical elements (mirrors) which cause losses. Moreover, a mercury lamp, which is sensitive to a magnetic field, is in this layout placed as far as possible from the magnet.

The parallel beam propagating from the OUT 2 then enters the optical system, where is placed the 90° Off-Axis Parabolic Mirror from Thorlabs of diameter 76.2 mm and RFL = 228.6 mm (shown in Figure 3.8 (a) with all parameters). The parabolic mirror reflects the parallel beam from the spectrometer, changes its direction by 90° and focuses it to a focus point. This beam path was calculated in ZEMAX. The result of this calculation is depicted in 3D Layout window from ZEMAX in Figure 3.8 (a). The assumption was that the diameter of the parallel beam going from the spectrometer is 40 mm.
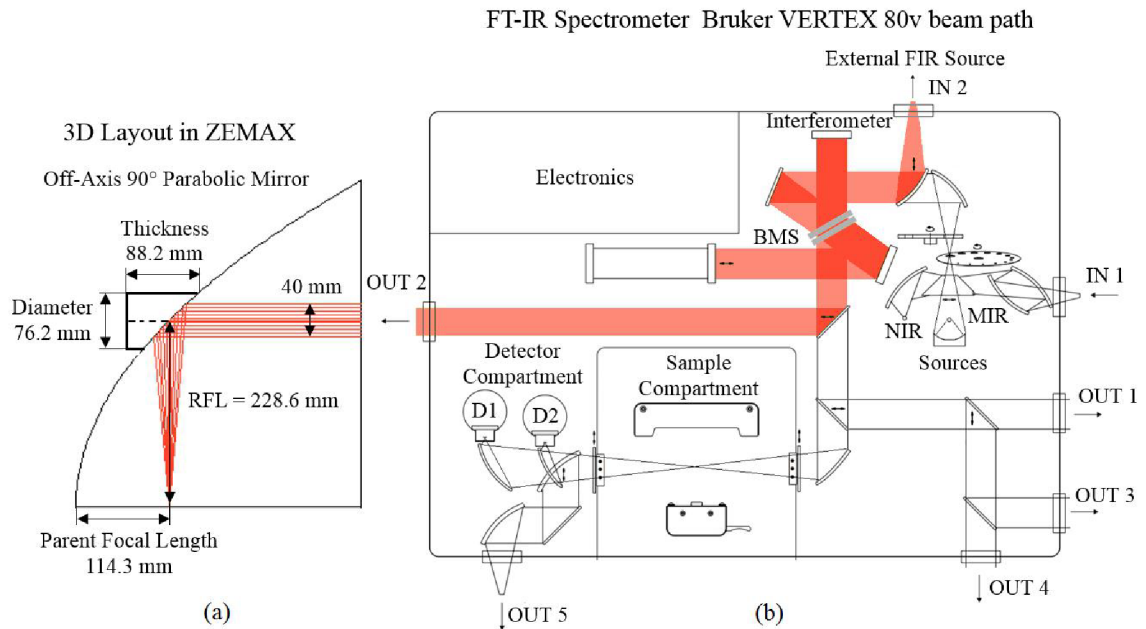
Figure 3.8: The beam path : (a) 3D Layout window from ZEMAX which shows the beam path (red) on the parabolic mirror with RFL = 228.6 mm, (b) schematic view of the FT-IR spectrometer Bruker VERTEX 80v with the beam path (red), adapted from [63].

The beam propagation through the whole improved magneto-optical setup, where all components are labeled and the beam is red, is shown in Figure 3.9. The parallel beam going from the spectrometer is reflected and focused by the parabolic mirror. From the optical system, it propagates to the first tube of the transmission probe, where it passes through the sample, which is inside of the superconductive magnet. At the end of the probe, it is reflected by two 90° mirrors 1, 2 and propagates to
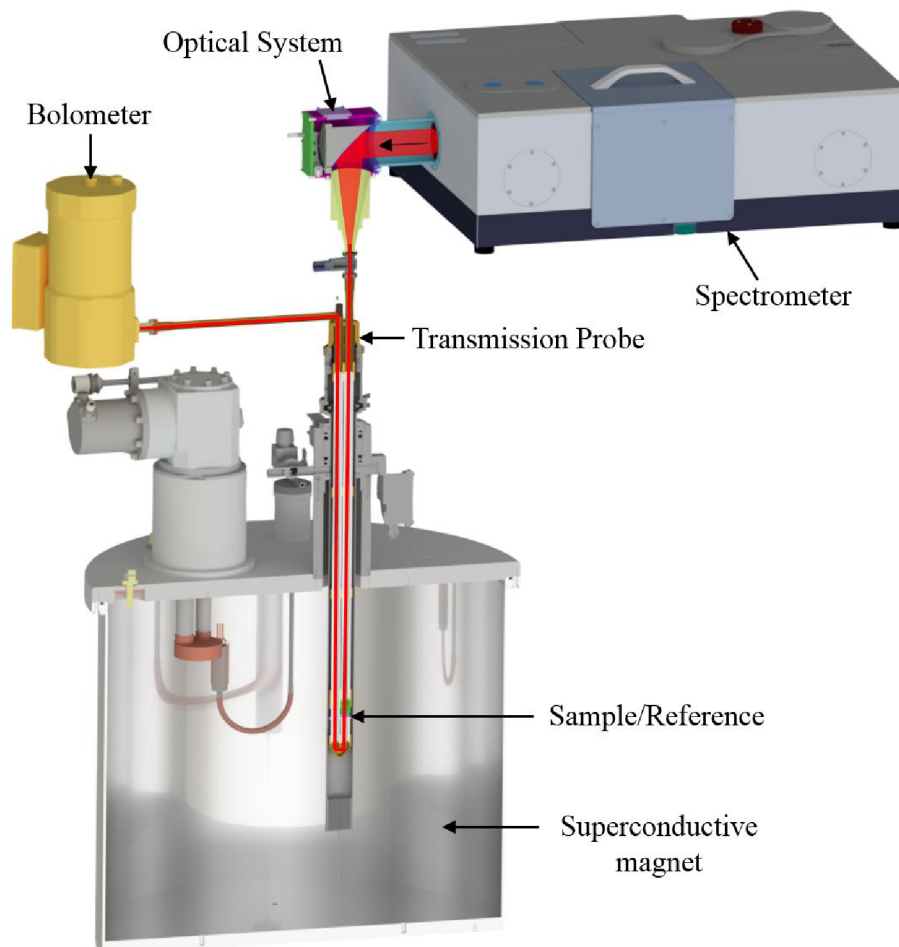
Figure 3.9: Schematic view of the beam propagation through the whole magneto-optical setup at CEITEC, where all components are labeled. The FIR beam propagating from the spectrometer through the optical system, the transmission probe inserted into the superconductive magnet to the bolometer is shown in red.

the second tube. At the end of second tube, 90° mirror 3 is located, which reflects it to the horizontal tube. From the horizontal tube, the beam is going straight to the bolometer. In the next subsections, the beam propagating through the individual components will be described in more details.

3.2.3 Optical System

The optical system is designed for guiding the beam from the spectrometer to the transmission probe. Figure 3.10 illustrates a labeled cross-section of the optical system (a) and a miniature 3D model of the optical system (b).

It is installed on the OUT 2 opening of the spectrometer. The original lid from this opening was removed and replaced by an aluminium tube with the flange at
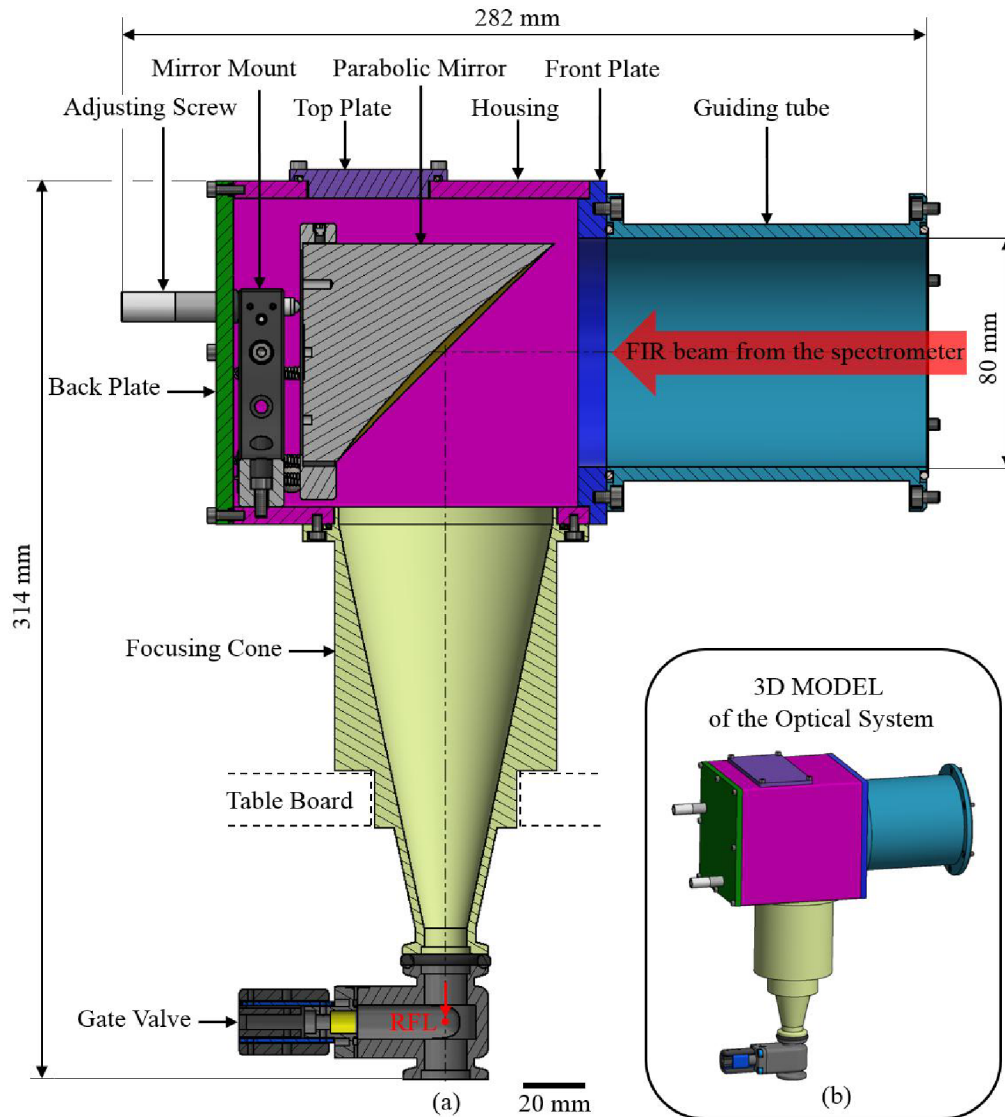
Figure 3.10: Schematic figure of the optical system: (a) a cross section of the optical system with a scale where all mentioned components are labeled and a direction of the beam is shown, (b) a miniature 3D model of the optical system.

the end, which has the same diameter, o-ring and six screw clearance holes for six screws as the original lid. The tube has the inner diameter of 80 mm. The opposite side of the tube is finished by the identical flange with o-ring and six clearance holes for screws which are mounted to the front plate of the housing. The front plate has an opening with the diameter of 80 mm and it is welded to the housing. The housing is made of aluminium square tube with the length of 125 mm, outside dimension (OD) = 120 mm and wall thickness of 6 mm.

In the housing, Thorlabs $\varnothing$3" 90° Off-Axis Parabolic Mirror (RFL = 228.6 mm)

with gold coating is implemented to reflect the beam and rotate it by 90°. It is inserted in the Thorlabs Precision Kinematic Mirror Mount, which is installed in the housing by two screws. It comprises two 1/4"-80 lockable adjusting screws which offers ±4° angular adjustment of the mirror. For these adjusting screws, two sealing openings in the back plate of the housing are formed. Removable knobs of the adjusting screws are replaced by Thorlabs spanner wrenches with o-rings in order to provide vacuum tightness around these openings in the back plate. The back plate is mounted on the housing by eight screws and there is a square-shaped rubber gasket between them. On the top of the housing, an opening for eventual manipulation with the mirror is created. It is covered by a removable top plate that is mounted to the housing with four screws. In order to secure a smooth transition of the beam reflected from the parabolic mirror to the transmission probe (see subsection 3.2.4), the focusing cone is used. In the bottom side of the housing, an opening for this cone is formed. In this opening, the focusing cone with the input diameter of 75 mm and the output diameter of 15 mm is inserted and installed with six screws. Its upper part is designed to have also bigger outside diameter than the rest because then it is possible to insert it to the cut out in the bourd of the movable table (see Figure 3.7). The optical system is then supported by the table plate and the wall of the spectrometer is not so loaded by the weight of the optical system. The end of the focusing cone is finished by DN25 KF flange. In order to separate the optical system and the transmission probe, which is after inserting to VTI filled with cryogenic helium gas, the gate valve is used. Unlike the previous setup, a smaller gate valve – aluminium mini gate valve VATLOCK from VAT [64] of inner diameter 15.1 mm with manual actuator (toggle lever) and DN25 KF flanges on both sides – is placed at the end of the optical system. By one DN25 KF flange, it is installed to the focusing cone and by another, it is mounted to the transmission probe (subsection 3.2.4). Up to the gate valve, the spectrometer with the optical system is placed under the rough vacuum by the pump of the spectrometer to reduce radiation losses. The focal point of the parabolic mirror is designed to be right in the middle of the gate valve from which is propagating to the transmission probe. All designed components in the optical system are made of aluminium and they will be covered by a black coating layer by anodizing due to same reasons as stated in the previous setup.

3.2.4 Transmission Probe

The transmission probe guides the beam from the optical system to the super-conductive magnet where it passes through a sample and then propagates to the bolometer. Figure 3.11 shows a cross-section of the whole probe with a scale, labeled components, and the beam propagation (red arrow) (a), a detail cross-section of

the upper part of the probe (b), an upper view of extreme positions of the sample holder (c), a detail cross-section of the parts around the sample holder (d), and 3D model of the transmission probe (e). Screws are not labeled for the sake of clarity.

In comparison with the previous setup, this transmission probe has a bigger diameter of the VTI (50 mm), its total length is shorter, and it is possible to measure sample and reference at the same conditions.

The upper part of the transmission probe (Figure 3.11) contains three brass tubes with the inner diameter of 15 mm. The brass tube 1 has the entrance tube mounted on its top for connecting the probe with the optical system, specifically with the gate valve (see subsection 3.2.3) by DN25 KF flange. The focused beam from the gate valve enters the probe by passing through the window which is part of the modified DN25 KF centering ring (Figure 3.11 (b)). The centering ring consists of two rings, inner and outer. The window is made from of a suitable material (mylar, polyethylene or polypropylene film) which is pressed and tensed between these two rings. The outer ring has a groove for o-ring and outer thread, which is screwed to the inner wall of the entrance tube to secure the position of the centering ring on the probe.

The brass tubes 1 and 2 are installed to the probe head. The position of these brass tubes inside the probe head is centered by a probe head plate which is mounted to the probe head by two screws. Two openings for connectors are created in the probe head, on which two connector plates are screwed, each with four screws. The probe head is attached to the magnet by inserting to the airlock[8].

Ends of the brass tubes 1 and 2 are inserted into the upper probe holder. To the opposite side of the upper probe holder, polished non-magnetic stainless steel tubes 1 and 2 are mounted. There are more probe holders which hold the proper position of tubes, two smaller - probe holders 1, 2 and bottom one – bottom probe holder. All tubes are fixed in the probe holders by together 56 grub screws. Around the tubes in the probe holders, squeezing rings are placed to secure the tubes and avoid their damage by screwing. On each probe holder, probe center plates 1, 2, 3, 4 are put for centering the tubes but mainly for a centering the sample holder rod and also for a heat exchange. The sample holder rod with the diameter of 3 mm is used for switching of the sample holder between two openings, sample or reference. The rod is controlled by a rod wheel placed above the probe head which is fixed to the rod with one screw. There is a hole made in the wall of the probe head for the sample holder rod which is equipped with several o-rings. This hole is covered by a rod plate installed to the wall of the probe head with two screws.

---

[8]device that permits passage between regions of differing pressures and environments
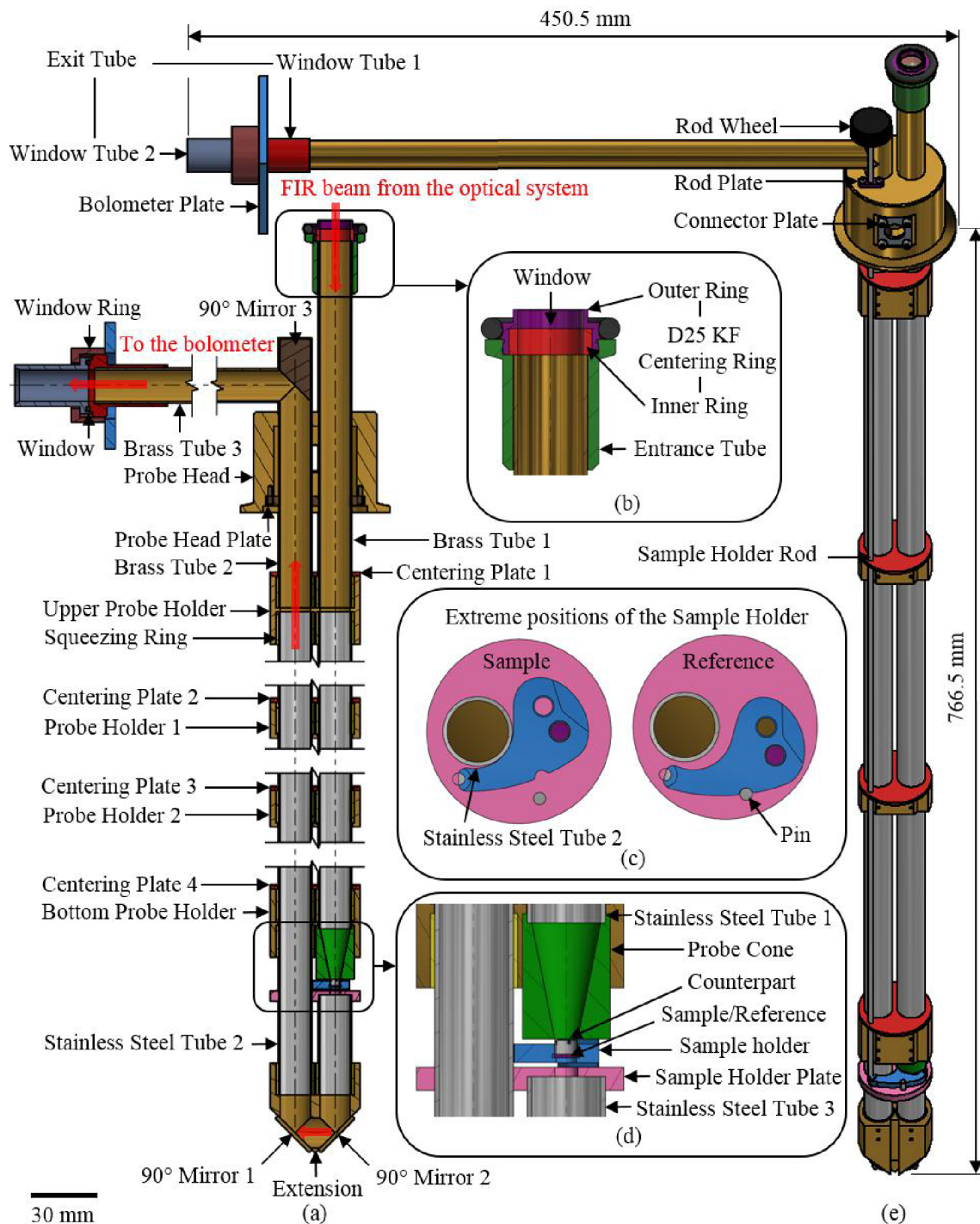
Figure 3.11: Schematic figure of the transmission probe: (a) a cross section of the whole probe with a scale, where all mentioned components are labeled and a propagation of the beam is shown (red arrow), (b) a detail cross section of the entrance tube with D25 KF centering ring, (c) an upper view of extreme positions of the sample holder, in sample configuration – extreme position is secured by the stainless steel tube 2 and in the reference configuration – extreme position is secured by the pin, (d) a detail cross section of the parts around the sample holder and (e) 3D model of the transmission probe. Screws are not labeled for the sake of clarity.

The beam propagating through the brass tube 1, stainless steel tube 1 then enters the probe cone, which is installed in the bottom probe holder. This cone is used for a smooth transition and focus of the beam from the tube of inner diameter 15 mm to a diameter of 5 mm, which is the diameter of a sample – 5 mm pressed powder pellet. Due to sample/reference problem in the first setup, the sample holder for sample and also reference at the same time is created. A sample is placed in one of two slots in the sample holder, another opening is left empty to provide measurement of a reference. The sample holder with the sample/reference in Faraday geometry is designed to be in the center of the magnetic field of the superconductive magnet. In this setup, sample is fixed in the sample holder with its counterpart, according to the problem with a flipped sample which has occurred in the first setup. The shape of the sample holder is designed to provide precise switching between sample and reference. On the one side, a pin is slotted to the sample holder to secure one extreme position and the second extreme position is secured by stainless steel tube 3 (see Figure 3.11 (c)). To provide rotation of the sample holder, the rod is mounted to the sample holder with a screw. Under the sample holder, the sample holder plate is placed, on which the sample holder is sliding by a small protrusion. Stainless steel tube 3 is inserted to the sample holder plate from the bottom side, from its the upper part, the sample holder rod is inserted. There is a hole with the diameter of 5 mm formed in the sample holder plate for the beam transmitted through the sample/reference. After the beam passes through the sample/reference, it is guided by a stainless steel tube 3 (Figure 3.11 (d)) to the extension, which connects both ends of the stainless steel tubes 2, 3. In the extension, there are two small 90° mirrors 1, 2 installed at the bottom of the extension, each with two screws. These mirrors reflect and guide the transmitted beam from the stainless steel tube 3 through the extension to stainless steel tube 2 (the transmitted beam makes a U-turn by these two mirrors). Then it is led by stainless steel tube 2 and brass tube 2 to another 90° mirror 3 located at the end of the brass tube 2. The beam is from this mirror reflected and propagates through the horizontal brass tube 3 through another window placed in the exit tube. The exit tube consists of the two parts – window tubes 1 and 2, between which the film of suitable material is situated. These parts are connected together by the window ring with inner thread. After the beam passes through this second window, it is going straight to the bolometer. To avoid the bolometer problem from the previous setup, the bolometer plate is mounted on the exit tube and then installed to the bolometer in order to secure the mutual position of the bolometer and the transmission probe.

4   Experimental part

In this chapter, the performance of the already assembled magneto-optical setup located at Institute of Physical Chemistry (IPC) at the University of Stuttgart together with the first magneto-optical measurements is presented. Putting the setup into the operation, tests and measurements were carried out with the collaboration of Ing. Antonín Sojka and M.Sc. Heiko Bamberger. Example of the magneto-optical spectra in the FIR range of SMM, based on transition metal - cobalt, will be provided. Additionally, FIR magneto-optical measurements from Grenoble High Magnetic Field Laboratory (GHMFL) at French National Center for Scientific Research (CNRS) will be shown. These measurements were carried out with the collaboration of RNDr. Milan Orlita, Ph.D. and Dr. Iris Crassee. By these measurements, the importance of the FIR spectroscopy in high magnetic field method in the field of molecular magnetism will be demonstrated and explained.

4.1   Testing of the setup

Before the testing of the first magneto-optical setup built at IPC (see section 3.1), it was necessary to pre-pump the Infrared Laboratories bolometer (order of 10^{-6} mbar) and properly fill it with liquid nitrogen (N_2) and helium (He). After all parts of the setup have been assembled, testing of the setup was carried out.

First of all, the spectrometer and optical system were up to the mylar window evacuated. Then, the system was probed by the red laser beam going from the spectrometer. After a small red spot was observed on the paper in the front of the probe tube going to the bolometer, the bolometer was moved as close as possible to the exit tube of the probe and the external Hg-Arc lamp was switched on. Then, a very weak signal detected by the bolometer was observed in the software OPUS[1] on the computer. In order to increase amplitude of the signal intensity, off-axis 90° parabolic mirror in the optical system was aligned by adjusting screws. By this alignment, the amplitude has significantly increased. Afterwards, also mirrors of the reflection unit placed in the sample compartment were aligned, which also considerably helped. To obtain an even better signal, the best position of the bolometer with the probe end was set. The best signal after the alignment, which was obtained for empty sample holder (without sample), had an amplitude around 5000 a.u. (with a gain factor of 5), see Figure 4.1 (a) obtained from software OPUS. The signal obtained for the sample (cobalt pellet) placed in the sample holder had an amplitude

---

[1]leading spectroscopy software for state-of-the-art measurement, processing and evaluation of IR spectra [65]

around 1324 a.u., which is shown in Figure 4.1 (b). This figures present a typical interferogram which was shown in Figure 2.2.
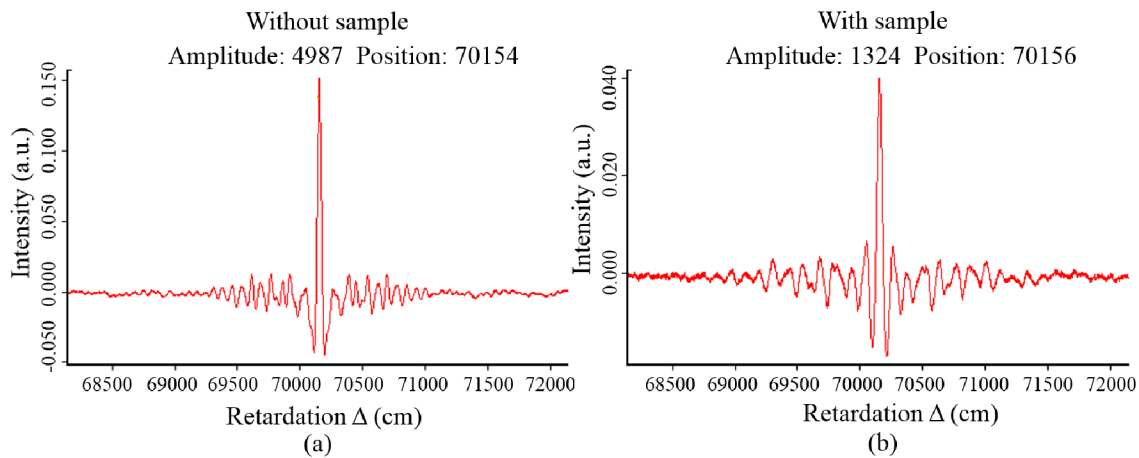

Figure 4.1: Amplitude of the signal in software OPUS: (a) for the sample holder without sample and (b) for the sample holder with sample.

An amplitude of the signal was influenced by evacuating the system and lowering the temperature. Before evacuating the spectrometer, the amplitude was 3580 a.u., after evacuating 4360 a.u. and after cooling down to 5 K it was 5280 a.u. For comparison, an amplitude of the signal, when the beam was not propagating through the coupling (only in the spectrometer and without sample), was measured around 17400 a.u. This implies that around 70% of the signal is lost by coupling and only 30% of the signal reaches the detector. But this result was to be expected. In every coupling like this, the losses inevitably occur. In our case, it is happening probably because the beam propagating from the reflection unit is not parallel, transmission probe is quite long, the probe is not secured to the bolometer, etc. So there is definitely a room for improvements in this setup. Nevertheless, almost a third of the signal is detected by the bolometer, so it is still possible to measure and obtain usable results.

4.2   Influence of number of scans

As stated in subsection 2.6.2, the important quantity defining the accuracy of the measurement is the signal-to-noise ratio. Therefore, the resolution of the spectra can be improved by taking a higher number of scans – the accumulation of spectra. This procedure significantly increases the signal-to-noise ratio by a factor equivalent to the square root of the number of scans [49]. For example, 64 accumulated scans would increase the resolution by a factor of eight.

To verify this fact, the empty sample holder in zero magnetic field, frequency range of $30 - 670 \, \text{cm}^{-1}$, temperature $5 \, \text{K}$ and with a resolution of $2 \, \text{cm}^{-1}$ was measured by different numbers of scans: 32, 64, 128, 256 (see Figure 4.2).
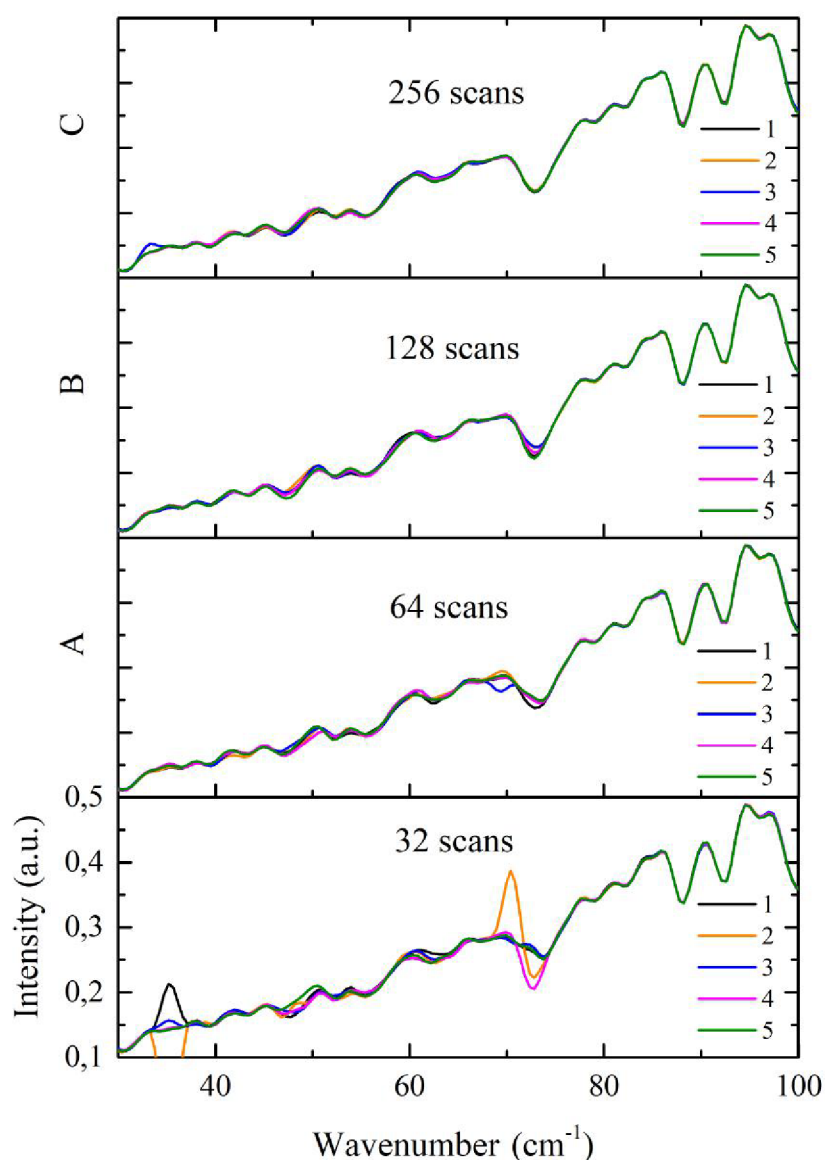

Figure 4.2: Influence of number of scans on a quality of the spectra. Measurement of each number of scans was repeated 5 times – colorful lines marked by 1 to 5 in legend. By increasing number of scans from 32 scans to A = 64 scans, B = 128 scans, C = 256 scans, it is obvious that with higher number of scans, spectrum is less noisy comparing to spectrum with lower number of scans.

Each measurement with a certain number of scans was repeated 5 times to distinguish where the noise occurs. The noisiest area of the spectra was below $100\,\mathrm{cm}^{-1}$, therefore Figure 4.2 focuses only on this relevant area. From Figure 4.2, it is obvious that with a higher number of scans, the spectrum is less noisy compared to the spectrum with a lower number of scans. It also implies that measurement in the region below $100\,\mathrm{cm}^{-1}$ is reproducible only with a higher number of scans. This result is important for samples which have field dependence expected in the region from 30 to $100\,\mathrm{cm}^{-1}$.

4.3   Influence of mylar windows

The influence of mylar films used in the magneto-optical setup was investigated in order to find out how they affect the quality of spectra. Films of two different thickness were tested. The film was mounted on the holder in the sample compartment and then the spectrum was recorded. It is shown in the Figure 4.3. Spectra for thick and thin foil were basically the same, just an intensity of the signal was stronger for thinner foil. For comparison, there is also background spectrum and spectrum of empty sample holder. Strong absorption peaks around $380\,\mathrm{cm}^{-1}$ and also at 440 and $510\,\mathrm{cm}^{-1}$ were observed in the spectra of both mylar films. The same features were recognized in the spectra of empty sample holder. Therefore, it is highly probable that these lines in the sample holder spectra are caused by the presence of the strong absorption lines of mylar film. This assumption can be confirmed also by literature: a major disadvantage of mylar window is the presence of a number of strong absorption lines between 400 and $2000\,\mathrm{cm}^{-1}$ [60] and the line at $380\,\mathrm{cm}^{-1}$ is the strongest absorption line of mylar in the far-infrared range according to [66]. Therefore, it is convenient to consider the changing of the window according to which spectral range will be observed. An alternative to the mylar may be already mentioned polypropylene, which has less and weaker absorption peaks below $2000\,\mathrm{cm}^{-1}$ and especially below $800\,\mathrm{cm}^{-1}$ than mylar. Another option can be polyethylene window, which is also used in such applications.

In Figure 4.3, sharp peaks in the area below $350\,\mathrm{cm}^{-1}$ in the empty sample holder spectrum are clearly visible and they are not observable in the spectra for mylar films and background. These peaks are probably caused by the atmosphere absorption, which has occurred somewhere in the coupling (the optical system or the transmission probe). Source of this problem can be the air gap between the probe end and the bolometer or the coupling is not completely vacuum tight.
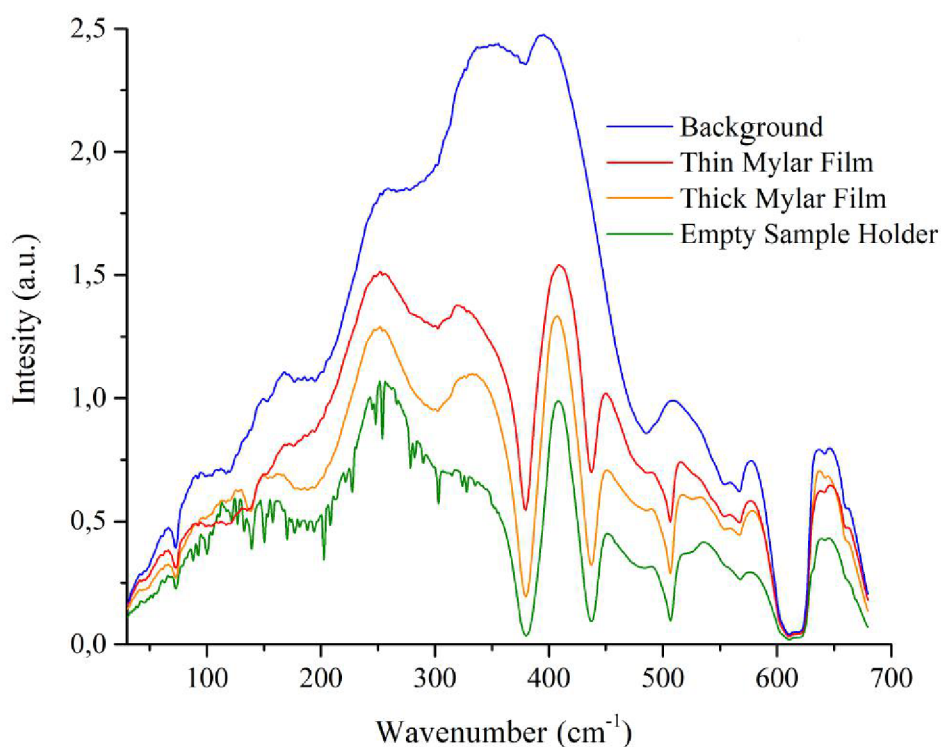
Figure 4.3: Influence of the mylar windows: strong absorption peaks in the mylar film spectra are observed around $380\,\mathrm{cm^{-1}}$ and also at 440 and $510\,\mathrm{cm^{-1}}$. The same peaks are recognized in the spectra of the empty sample holder. It is caused most probably by the two mylar windows used in the transmission probe. Sharp peaks in the area below $350\,\mathrm{cm^{-1}}$ in the empty sample holder spectrum are caused probably by the air absorption. Possible sources of the air absorption are air gap between the probe end and the bolometer or the coupling (the optical system and the transmission probe) is not completely vacuum tight.

4.4   Sample preparation

All measured samples were prepared at IPC as pressed powder pellets using special equipment, dry pellet pressing die set and its accessories shown in Figure 4.4 (a) and manual hydraulic dry pressing machine shown in Figure 4.4 (b). Measured pellets (based on transition metals) were dispersed in eicosane[2] (ratio sample to eicosan usually 1:10) in order to make samples more transparent for the FIR beam and thus to obtain better transmitted signal.

---

[2]$C_{20}H_{42}$

(a)   (b)
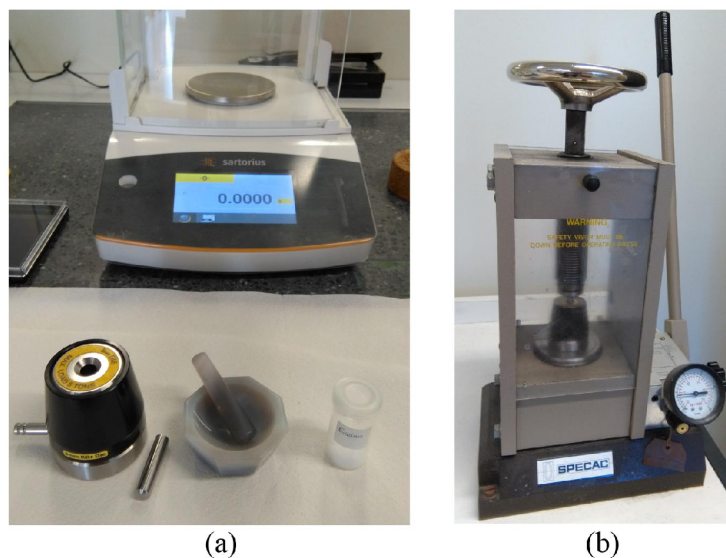
Figure 4.4: Equipment for pressed powder pellets preparation at Institute of Physical Chemistry (University of Stuttgart): (a) dry pellet pressing die set and its accessories and (b) manual hydraulic dry pressing machine.

4.5 Magneto-optical measurement in Stuttgart

Relative transmission spectra of the cobalt sample $K_2[Co(L_2^-)_2]$ (**1**) shown in Figure 4.5, where H_2L = 1,2-bis(methanesulfonamido)benzene, were acquired on the magneto-optical setup at IPC in Stuttgart (3.1) in the frequency range of $30-670\,cm^{-1}$ with the resolution of $2\,cm^{-1}$, temperature $5\,K$ and for 64 scans. Amplitude of the signal was during the whole measurement predominantly stable, around $1320\,a.u.$ Magnetic fields were applied up to $15\,T$ in Faraday geometry.

Figure 4.5: Crystallographic structure of the $K_2[Co(L_2^-)_2]$. Cobalt is shown in blue, oxygen in red, sulfur in yellow, nitrogen in violet and carbon in grey, hydrogen atoms are omitted for clarity. Provided by Heiko Bamberger.

The sample was synthesized by M.Sc. Uta Frank from the group of Biprajit Sarkar. During the preparation of the pellet, the sample was diluted with eicosane and then 11% (89% of eicosane) pressed powder pellet with the weight of 16.7 mg and the diameter of 8 mm was created. Far-infrared transmission spectra (Figure 4.6) in dif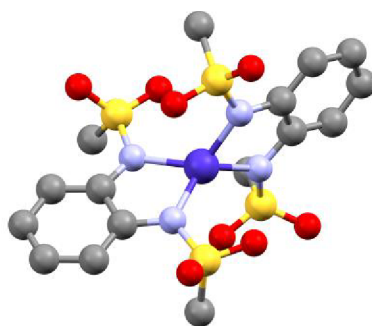ferent magnetic fields (0 T — 15 T with the step of 3 T) were recorded to determine the zero-field gap ($2D$). Due to the absence of sample holder for sample and reference, it was not possible to record typical transmission spectra. Therefore, relative transmission spectra $T_R(B)$ was calculated by dividing each magnetic field spectrum $T(B)$ by second zero field measurement $T(0)$, which was measured at the end.

4.5.1   Results and Discussion

Figure 4.6 (a) shows recorded spectra on pressed powder pellet of **1** dispersed in eicosane in the frequency range of $100-400\,\mathrm{cm}^{-1}$ where is clearly visible which peaks are field dependent and which are not. These spectra have shown a clear field dependence in the region around $230\,\mathrm{cm}^{-1}$ due to features which grow with the increasing magnetic field. Such behavior is not observed in other places in this spectra. For better visibility, the field-dependent features are enlarged in Figure 4.6 (b) in the frequency range of $160-300\,\mathrm{cm}^{-1}$.

The field-dependent features are attributed to the EPR transition from $m_S = \pm 3/2$ to $m_S = \pm 1/2$ (total spin of the **1** is $S = 3/2$). This measurement has demonstrated the presence of a very high zero-field gap of approximately $230\,\mathrm{cm}^{-1}$ corresponding to $|\,D\,| = 115\,\mathrm{cm}^{-1}$ (in the absence of a rhombic ZFS term).

By this FIR transmission measurement in the high magnetic field has been tested the performance of the magneto-optical setup at IPC and simultaneously, it proved that this setup is capable of providing reasonable spectra and results.
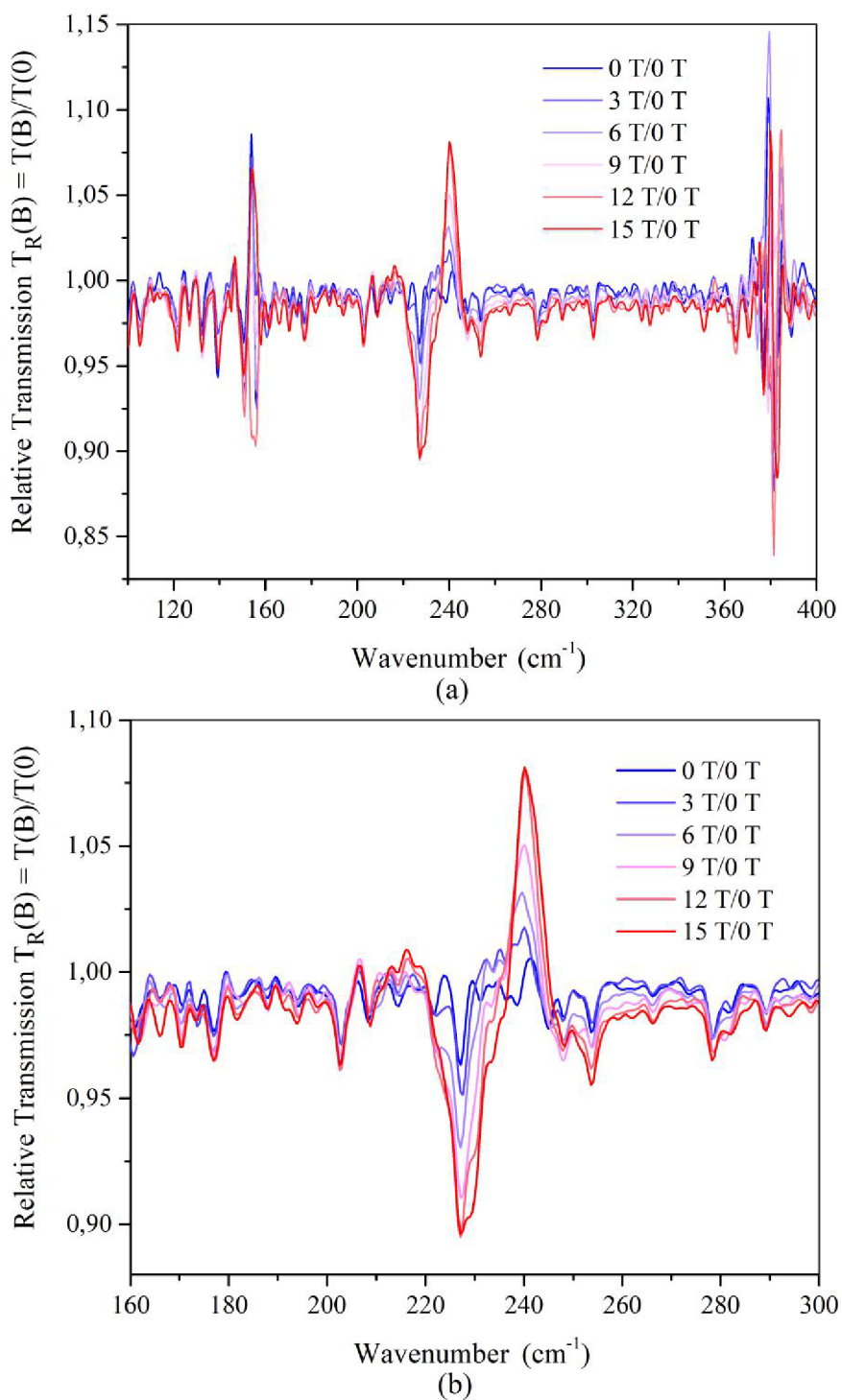
Figure 4.6: Far-infrared spectra recorded on pressed powder pellet of 11% **1** dispersed in 89% eicosane. (a) In the spectra is clearly visible which features are field-dependent and which are not. The field dependence is observed in features which grow with the increasing magnetic field in the region around $230\,\mathrm{cm}^{-1}$, (b) enlarged of the field-dependent features at $230\,\mathrm{cm}^{-1}$. The relative transmission spectra $T_R(B)$ was calculated by dividing each magnetic field spectrum $T(B)$ by second zero field measurement $T(0)$.

4.6 Magneto-optical measurement in Grenoble

Relative transmission spectra of the cobalt sample $[Co(2NH_2\text{-}3CH_3\text{-}py)_2(ac)_2]$ (**2**) (Figure 4.7), where $(2NH_2\text{-}3CH_3\text{-}py)$ is 2-amino-3-methylpyridine and (ac) is acetate anion, were obtained on the magneto-optical setup at GHMFL in Grenoble in the frequency range of $0-2500\,cm^{-1}$ with the resolution of $3\,cm^{-1}$, temperature $2\,K$ and for 256 scans. Magnetic fields were applied up to $11\,T$ in Faraday geometry. The setup at GHMFL consists of Bruker IFS 66v/s FTIR spectrometer with a Hg-Arc lamp source, where the sample is placed inside the 11 T solenoid magnet, with a composite bolometer detector element located inside the magnet.
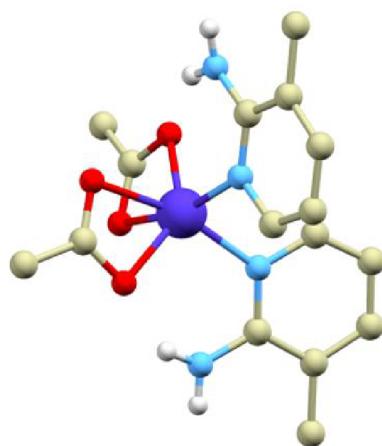
Figure 4.7: Crystallographic structure of the $[Co(2NH_2\text{-}3CH_3\text{-}py)_2(ac)_2]$. Cobalt is shown in dark blue, nitrogen in light blue, oxygen in red, carbon in yellow and hydrogen in white. Provided by Ivan Nemec.

The sample was synthesized by Ing. Ivan Nemec, Ph.D. from Palacký University in Olomouc. During the preparation of the pellet, the sample was diluted with eicosane and then 9% (91% of eicosane) pressed powder pellet with the weight of $17.5\,mg$ and the diameter of $5\,mm$ was created. Far-infrared transmission spectra (Figure 4.8) in different magnetic fields ($1\,T$ — $11\,T$ with the step of $1\,T$) were recorded to determine the zero-field gap ($2D$). The setup in Grenoble has the sample holder designed for sample together with reference, which allows calculating of classical transmission spectra. However, we will present here only the relative transmission spectra calculated by dividing each magnetic field spectrum $T(B)$ by the zero field measurement $T(0)$, for the consistency with the previous measurement.

4.6.1   Results and Discussion

Figure 4.8 (a) shows recorded spectra on pressed powder pellet of **2** dispersed in eicosane in the frequency range of $30-100\,\mathrm{cm}^{-1}$ where the field-dependent features, moving with increasing magnetic field to the right, are fitted and highlighted by a black line. The point where the line crosses the x-axis can be considered as the zero-field gap $(2D)$ value. In this spectra, the line is crossing x-axis approximately at $44\,\mathrm{cm}^{-1}$ which then corresponds to $\mid D \mid = 22\,\mathrm{cm}^{-1}$ (in the absence of a rhombic ZFS term). The field-dependent features are attributed to the EPR transition from $m_S = \pm 3/2$ to $m_S = \pm 1/2$ (total spin of the sample is S = 3/2). Figure 4.8 (b) illustrates schema of Kramers doublets for **2**. This energy-level structure serves for better understanding of the spectra in Figure 4.8 (a). Red arrow represents the value where the black line crosses the x and green arrows represents the x-axis value for the point where the black line crosses the 5 T and 10 T spectrum.

On the pellet **2**, traditional MW EPR spectra were recorded on HF-EPR spectrometer at IPC in Stuttgart. Based on the calculation and simulations of the obtained EPR data made by Dr. Vinicius Santana, $D = 22\,\mathrm{cm}^{-1}$. This result is in very good agreement with the result from the previous FIR measurement. Therefore, FIR spectroscopy in magnetic field spectra can be used for confirmation of the results from traditional EPR. By this measurement we want to point out the importance of the FIR spectroscopy in magnetic field method in the field of molecular magnetism.

The key parameter for determining properties and potential of SMMs, is the parameter D. Therefore, the majority of the techniques for investigation of SMMs are trying to determine the value of D. For example, in traditional EPR spectroscopy, it is done by simulating the obtained data. Due to the sometimes complicated interpretation of traditional EPR measurements, other measurement techniques are desirable. Ideal method for this purpose is FIR spectroscopy in magnetic field, which can yield precise determination of the energy-level structure and thus has the advantage to determine this value directly from the spectra. Moreover, this technique is in particular suitable for SMMs with very large ZFS, mainly based on transition metal complexes or lanthanides, in which commonly used EPR spectrometers do not provide experimental access to the magnetic resonance transitions. In other words, this method allows to study EPR by the use of FIR region, lying adjacent to MW, and thus broaden a commonly used MW range for investigation of SMMs.

(a)

(b)
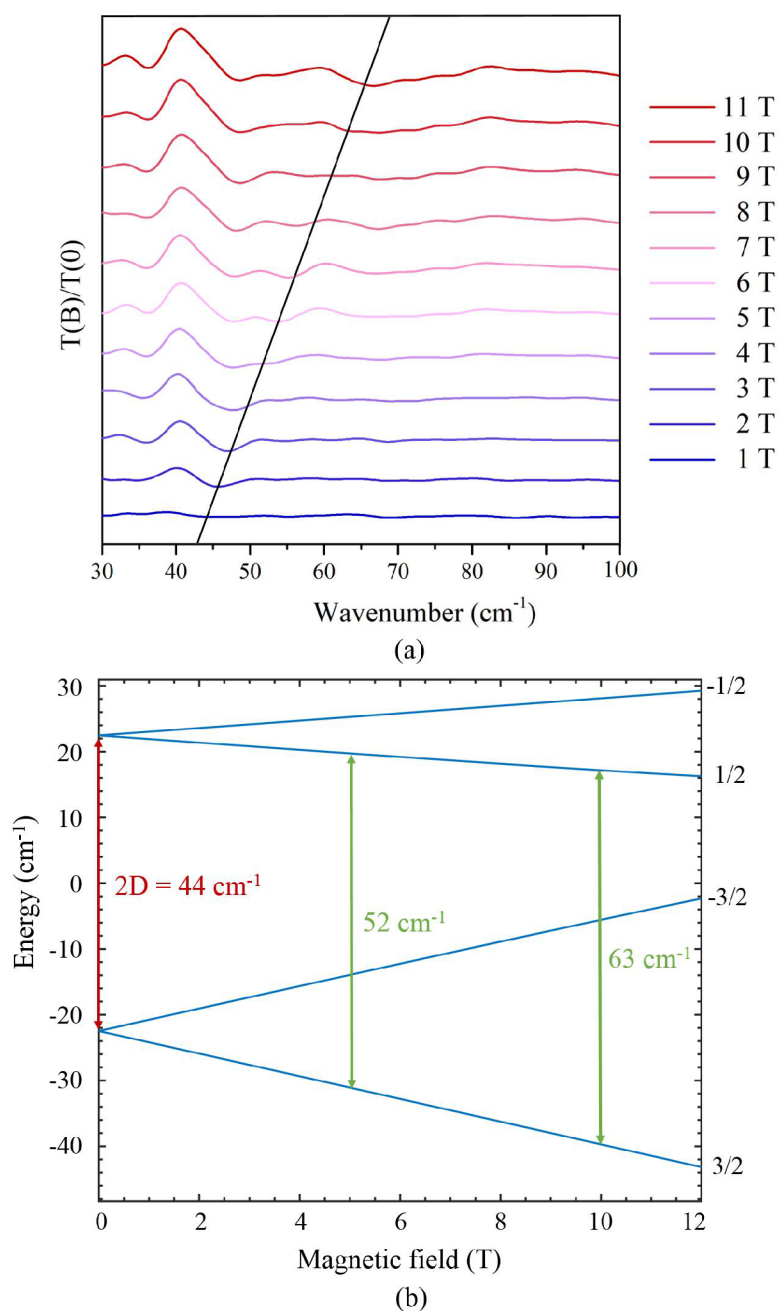
Figure 4.8: Far-infrared spectra recorded on pressed powder pellet of 9% **2** dispersed in 91% eicosane. (a) The point where the line crosses the x-axis can be considered as the zero-field gap ($2D$) value, which is here approximately at $44\,\mathrm{cm^{-1}}$. (b) Schema of Kramers doublets for **2**. This energy-level structure serves for better understanding of the spectra in Figure 4.8 (a). Red arrow represents the value where the black line crosses the x, first green arrow represents the x-axis value for the point where the black line crosses the $5\,\mathrm{T}$ spectrum and second green arrow represents the x-axis value for the point where the black line crosses the $10\,\mathrm{T}$ spectrum.

Summary and outlook

The main goal of the thesis was to design the setup of the FT-IR spectrometer coupled to superconductive magnet to mediate the method of the FIR spectroscopy in the high magnetic field. This method presents a very important tool in the characterization of various materials including Single-Molecule Magnets (SMMs). The setup allows studying magnetic resonance phenomena such as EPR through the use of the FIR spectroscopy.

First two chapters provide theoretical background necessary for the understanding of the problematics. The first chapter is dedicated to molecular magnetism, especially to SMMs, the important target group for investigation by this method. The second chapter sheds light on the FIR spectroscopy and shows existing magneto-optical setups across the world.

The third chapter is dedicated to the design of magneto-optical setups itself. Two designs of the setups, in which FT-IR spectrometers are coupled to superconductive magnets were described in detail. The first described setup, designed during the internship at IPC in Stuttgart, is already assembled. The second magneto-optical setup draws on the experiences gained in the first setup and is designed for CEITEC. By comparing these two designs, the setup for CEITEC is improved version of the IPC setup. For example, it is capable to provide measurements of sample and reference at the same conditions thanks to the sample holder designed for switching between two slots. Additionally, adjustment of the setup and sample exchange is easier because this setup is implemented on the automatically driven table.

The fourth chapter provides experimental results obtained from two different magneto-optical setups. The first described results were obtained on the already assembled magneto-optical setup at IPC in Stuttgart. In the beginning, the performance of this setup was examined. Factors which affect the signal quality, such as choice of the windows in the system, was identified. Moreover, it was found out that in some range of the spectra, it is possible to obtain reproducible results with the higher number of scans. Then, measurements of SMMs sample based on cobalt were performed in order to obtain FIR transmission spectra of the sample in the magnetic field up to $15\,\mathrm{T}$. These spectra have shown a clear magnetic field dependence in the region around $230\,\mathrm{cm}^{-1}$ attributed to the EPR transition. Therefore, this measurement has demonstrated the presence of a very high zero-field gap of approximately $230\,\mathrm{cm}^{-1}$ corresponding to $\mid D \mid = 115\,\mathrm{cm}^{-1}$, where D is the key parameter for determining properties and potential of SMMs. To sum up, by this FIR transmission measurement in the high magnetic field has been tested the performance of the magneto-optical setup at IPC and simultaneously, these measurements have proved that the setup is capable of providing reasonable and usable results.

Other experimental results were acquired at Grenoble High Magnetic Field Laboratory (GHMFL) at French National Center for Scientific Research (CNRS). The cobalt-based SMMs sample was measured in the magnetic field up to 11 T and FIR transmission spectra were obtained. The field-dependent features were observed in the spectra approximately at $44\,\mathrm{cm}^{-1}$ which then corresponds to $\mid D \mid = 22\,\mathrm{cm}^{-1}$. This result was compared with the value calculated based on the simulations retrieved from HF-EPR measurement data, which was $\mid D \mid = 22\,\mathrm{cm}^{-1}$. These results are in a very good agreement. Due to the sometimes complicated interpretation of traditional EPR measurements, other measurement techniques are desirable. It implies that the result from the FIR spectroscopy in the high magnetic field is very helpful for confirmation of the result from traditional EPR spectroscopy. Therefore, for proper investigation of SMMs, it is necessary to use multi-frequency EPR spectrometers and thus also setups of the FT-IR spectrometers coupled to a superconductive magnets which broaden typically used microwave range to FIR region, which is lying adjacent. By this measurement, the importance of the FIR spectroscopy in the high magnetic field method in the field of molecular magnetism was demonstrated. Also, the purpose of the magneto-optical setup designed in this thesis was justified.

To conclude, the FIR spectroscopy in the high magnetic field presents a very important tool in the characterization of materials such as SMMs. It allows studying EPR of SMMs with very large zero-field splitting, mainly based on transition metal complexes or lanthanides, in which commonly used EPR systems do not provide experimental access to the magnetic resonance transitions. In addition, applications of the FIR spectroscopy and the high magnetic field method is not limited to the investigation of SMMs, it can also probe and elucidate properties of novel 2D materials such as graphene. The investigation of 2D materials beside the SMMs by means of this method, which is mediated by the setup designed in the thesis, will certainly be a matter of interest in the future.

Bibliography

[1] The Digital Universe of Opportunities: Rich Data and the Increasing Value of the Internet of Things: Data Growth, Business Opportunities, and the IT Imperatives. *EMC Digital Universe with Research & Analysis by IDC* [online]. 2014 [cit. 2018-03-25]. Available from: `https://www.emc.com/leadership/digital-universe/2014iview/executive-summary.htm`

[2] CHILTON, N. How to store data on magnets the size of a single atom. *The University of Manchester Magazine* [online]. 2017 [cit. 2018-03-25]. Available from: `http://www.manchester.ac.uk/discover/news/how-to-store-data-on-magnets-the-size-of-a-single-atom/`

[3] WHAT IS MOLECULAR MAGNETISM?. *The European Institute of Molecular Magnetism* [online]. 2016 [cit. 2018-03-25]. Available from: `http://www.unizar.es/eimm2/tutorial/7.php`

[4] WINPENNY, R. and AROMÍ, G. *Single-molecule magnets and related phenomena.* New York: Springer, 2006. ISBN 3540332391.

[5] SESSOLI, R., GATTESCHI D., CANESCHI, A., *et al.* Magnetic bistability in a metal-ion cluster. *Nature* [online]. 1993, **365**(6442), 141-143 [cit. 2018-03-23]. DOI: 10.1038/365141a0. ISSN 0028-0836. Available from: `http://www.nature.com/doifinder/10.1038/365141a0`

[6] HAAS, S. *Far-infrared spectroscopy of lanthanide-based molecular magnetic materials.* 2015. Dissertation. University of Stuttgart. Available from: `https://elib.uni-stuttgart.de/handle/11682/5178`

[7] VAN SLAGEREN, J. *Introduction to Molecular Magnetism* [online]. Physikalisches Institut, Universität Stuttgart [cit. 2018-03-25]. Available from: `http://obelix.physik.uni-bielefeld.de/~schnack/molmag/material/123.pdf`

[8] GATTESCHI, D., SESSOLI, R. and CORNIA, A. Single-molecule magnets based on iron(iii) oxo clusters. *Chemical Communications* [online]. (9), 725-732 [cit. 2018-04-25]. DOI: 10.1039/a908254i. ISSN 13597345. Available from: `http://xlink.rsc.org/?DOI=a908254i`

[9] MISRA, S. K. *Multifrequency Electron Paramagnetic Resonance* [online]. Weinheim, Germany: Wiley-VCH Verlag GmbH & Co., 2011 [cit. 2018-03-25]. ISBN 9783527633531. Available from: `https://www.nap.edu/catalog/18355/high-magnetic-field-science-and-its-application-in-the-united-states`

[10] WOODRUFF, D. N., WINPENNY, R. E. P. and LAYFIELD, R. A. Lanthanide Single-Molecule Magnets. *Chemical Reviews* [online]. 2013, **113**(7), 5110-5148 [cit. 2018-04-25]. DOI: 10.1021/cr400018q. ISSN 0009-2665. Available from: `http://pubs.acs.org/doi/10.1021/cr400018q`

[11] SESSOLI, R., TSAI, H. L., SCHAKE, A. R., *et al.* High-spin molecules: [Mn12O12(O2CR)16(H2O)4]. *Journal of the American Chemical Society* [online]. 1993, **115**(5), 1804-1816 [cit. 2018-04-25]. DOI: 10.1021/ja00058a027. ISSN 0002-7863. Available from: `http://pubs.acs.org/doi/abs/10.1021/ja00058a027`

[12] FROST, J. M., HARRIMAN, K. L. M. and MURUGESU, M. The rise of 3-d single-ion magnets in molecular magnetism: towards materials from molecules?. *Chemical Science* [online]. 2016, **7**(4), 2470-2491 [cit. 2018-06-01]. DOI: 10.1039/C5SC03224E. ISSN 2041-6520. Available from: `http://xlink.rsc.org/?DOI=C5SC03224E`

[13] WECKHUYSEN, B. M., HEIDLER, R., SCHOONHEYDT R. A., *et al.Electron Spin Resonance Spectroscopy* [online]. 2004 [cit. 2018-04-01]. Mol. Sieves. 4. 2733-2733. DOI: 10.1007/b94238.

[14] LIDDLE, S. T. and VAN SLAGEREN, J. Improving f-element single molecule magnets. *Chemical Society Reviews* [online]. 2015, **44**(19), 6655-6669 [cit. 2018-04-25]. DOI: 10.1039/C5CS00222B. ISSN 0306-0012. Available from: `http://xlink.rsc.org/?DOI=C5CS00222B`

[15] BUSCHOW, K.H.J. *Concise encyclopedia of magnetic & superconducting materials.* 2nd ed. Amsterdam: Elsevier, 2005. ISBN 9780080457659.

[16] RECHKEMMER, Y., BREITGOFF, F. D., VAN DER MEER, M., *et al.* A four-coordinate cobalt(II) single-ion magnet with coercivity and a very high energy barrier. *Nature Communications* [online]. 2016, **7**, 10467- [cit. 2018-04-25]. DOI: 10.1038/ncomms10467. ISSN 2041-1723. Available from: `http://www.nature.com/doifinder/10.1038/ncomms10467`

[17] THOMAS, L., LIONTI, F.,BALLOU, R., *et al.* Macroscopic quantum tunnelling of magnetization in a single crystal of nanomagnets. *Nature* [online]. 1996, **383**(6596), 145-147 [cit. 2018-04-25]. DOI: 10.1038/383145a0. ISSN 0028-0836. Available from:`http://www.nature.com/doifinder/10.1038/383145a0`

[18] LAYFIELD, R. A. and MURUGESU, M. *Lanthanides and actinides in molecular magnetism.* Weinheim: Wiley-VCH, 2015. ISBN 978-3527335268.

[19] LU, J., GUO, M. and TANG, J. Recent Developments in Lanthanide Single-Molecule Magnets. *Chemistry - An Asian Journal* [online]. 2017, **12**(21), 2772-2779 [cit. 2018-04-25]. DOI: 10.1002/asia.201701032. ISSN 18614728. Available from: `http://doi.wiley.com/10.1002/asia.201701032`

[20] WALDMANN, O. A Criterion for the Anisotropy Barrier in Single-Molecule Magnets. *Inorganic Chemistry* [online]. 2007, **46**(24), 10035-10037 [cit. 2018-05-23]. DOI: 10.1021/ic701365t. ISSN 0020-1669. Available from: `http://pubs.acs.org/doi/abs/10.1021/ic701365t`

[21] NEESE, F. and PANTAZIS, D. A. What is not required to make a single molecule magnet. *Faraday Discuss* [online]. 2011, **148**, 229-238 [cit. 2018-04-25]. DOI: 10.1039/C005256F. ISSN 1359-6640. Available from: `http://xlink.rsc.org/?DOI=C005256F`

[22] BENELLI, C. and GATTESCHI, D. *Introduction to molecular magnetism: from transition metals to lanthanides*. Weinheim: Wiley-VCH, 2015. ISBN 9783527335404.

[23] Printable Chemistry Worksheets. *ThoughtCo.* [online]. [cit. 2018-04-25]. Available from: `https://www.thoughtco.com/printable-chemistry-worksheets-609242`

[24] ISHIKAWA, N., SUGITA, M., ISHIKAWA, T., *et al.* Lanthanide Double-Decker Complexes Functioning as Magnets at the Single-Molecular Level. *Journal of the American Chemical Society* [online]. 2003, **125**(29), 8694-8695 [cit. 2018-04-26]. DOI: 10.1021/ja029629n. ISSN 0002-7863. Available from: `http://pubs.acs.org/doi/abs/10.1021/ja029629n`

[25] GANIVET, C. R., BALLESTEROS, B., DE-LA-TORRE, G., *et al.* Influence of Peripheral Substitution on the Magnetic Behavior of Single-Ion Magnets Based on Homo- and Heteroleptic Tb III Bis(phthalocyaninate). *Chemistry - A European Journal* [online]. 2013, **19**(4), 1457-1465 [cit. 2018-04-25]. DOI: 10.1002/chem.201202600. ISSN 09476539. Available from: `http://doi.wiley.com/10.1002/chem.201202600`

[26] RINEHART, J. D. and LONG, J. R. Exploiting single-ion anisotropy in the design of f-element single-molecule magnets. *Chemical Science* [online]. 2011, **2**(11), 2078- [cit. 2018-04-25]. DOI: 10.1039/c1sc00513h. ISSN 2041-6520. Available from: `http://xlink.rsc.org/?DOI=c1sc00513h`

[27] SORACE, L., BENELLI, C. and GATTESCHI, D. Lanthanides in molecular magnetism: old tools in a new field. *Chemical Society Reviews* [online]. 2011,

40(6), 3092- [cit. 2018-04-25]. DOI: 10.1039/c0cs00185f. ISSN 0306-0012. Available from: `http://xlink.rsc.org/?DOI=c0cs00185f`

[28] HABIB, F. and MURUGESU, M. Lessons learned from dinuclear lanthanide nano-magnets. *Chemical Society Reviews* [online]. 2013, **42**(8), 3278- [cit. 2018-04-25]. DOI: 10.1039/c2cs35361j. ISSN 0306-0012. Available from: `http://xlink.rsc.org/?DOI=c2cs35361j`

[29] GOODWIN, C. A. P., ORTU, F., RETA, D., *et al.* Molecular magnetic hysteresis at 60 kelvin in dysprosocenium. *Nature* [online]. 2017, **548**(7668), 439-442 [cit. 2018-03-25]. DOI: 10.1038/nature23447. ISSN 0028-0836. Available from: `http://www.nature.com/doifinder/10.1038/nature23447`

[30] ARDAVAN, A., RIVAL, O., MORTON, J. J. L., *et al.* Will Spin-Relaxation Times in Molecular Magnets Permit Quantum Information Processing?. *Physical Review Letters* [online]. 2007, **98**(5), - [cit. 2018-04-26]. DOI: 10.1103/PhysRevLett.98.057201. ISSN 0031-9007. Available from: `https://link.aps.org/doi/10.1103/PhysRevLett.98.057201`

[31] MANNINI, M., PINEIDER, F., DANIELI, C., *et al.* Quantum tunnelling of the magnetization in a monolayer of oriented single-molecule magnets. *Nature* [online]. 2010, **468**(7322), 417-421 [cit. 2018-04-26]. DOI: 10.1038/nature09478. ISSN 0028-0836. Available from: `http://www.nature.com/articles/nature09478`

[32] *HGST Reaches 10-Nanometer Patterned-Bit Milestone, Nanotechnology Process Will Double Today-s Disk Drive Data Density* [online]. February 28, 2013. Available from:`http://www.hgst.com/company/media-room/press-releases/hgst-reaches-10-nanometer-patterned-bit-milestone-nanotechnology`

[33] *WD BLUE PC MOBILE HARD DRIVE: TECHNICAL SPECIFICATIONS* [online]. Available from: `https://www.wdc.com/products/internal-storage/wd-blue-mobile.html`

[34] JOHNSON, D. Single Atom Serves as World's Smallest Magnet and Data Storage Device. *IEEE Spectrum* [online]. 2017 [cit. 2018-03-25]. Available from: `https://spectrum.ieee.org/nanoclast/semiconductors/nanotechnology/single-atom-serves-as-worlds-smallest-magnet-and-data-storage-device`

[35] GATTESCHI, D., BARRA, A. L., CANESCHI, A., *et al.* EPR of molecular nanomagnets. *Coordination Chemistry Reviews* [online]. 2006,

250(11-12), 1514-1529 [cit. 2018-03-26]. DOI: 10.1016/j.ccr.2006.02.006. ISSN 00108545. Available from: `http://linkinghub.elsevier.com/retrieve/pii/S001085450600052X`

[36] WALKER, J., RESNICK, R. and HALLIDAY, D. *Halliday & Resnick fundamentals of physics.* 10th edition. Hoboken, NJ: Wiley, 2014. ISBN 978-1-118-23072-5.

[37] WEIL, J. A. and BOLTON, J. R. *Electron paramagnetic resonance: elementary theory and practical applications.* 2nd ed. Hoboken, N.J.: Wiley-Interscience, 2007. ISBN 978-0471-75496-1.

[38] WECKHUYSEN, B., HEIDLER, R. and SCHOONHEYDT, R. *Electron Spin Resonance Spectroscopy* [online]. 2004, , Mol. Sieves. 4. 2733-2733. DOI: 10.1007/b94238.

[39] HRUBÝ, J. *Preparation and Characterization of Graphene Based Hybrid Materials.* Brno, 2017. 91 p. Master-s thesis. Brno University of Technology. Faculty of Mechanical Engineering. Supervised by Ing. Petr NEUGEBAUER, Ph.D.

[40] DERRICK, M. R., STULIK, D. and LANDRY, J. M. *Infrared spectroscopy in conservation science.* Los Angeles: Getty Conservation Institute, 1999. ISBN 0-89236-469-6.

[41] CHRISTY, A. A., OZAKI, Y. and GREGORIOU, V. G. *Modern fourier transform infrared spectroscopy.* New York: Elsevier, 2001. ISBN 978-0444500441.

[42] STUART, B. *Infrared spectroscopy: fundamentals and applications.* Hoboken, NJ: J. Wiley, 2004. ISBN 0-470-85427-8.

[43] HAYNES, W. M. *CRC handbook of chemistry and physics: a ready-reference book of chemical and physical data.* 92nd ed. Boca Raton, FL: CRC Press, 2011. ISBN 1439855110.

[44] GRIFFITHS, P. R. and DE HASETH, J. A. *Fourier transform infrared spectrometry.* 2nd ed. Hoboken, N.J.: Wiley-Interscience, 2007. ISBN 978-0-471-19404-0.

[45] Optics 101: Level 1 Theoretical Foundations: THE ELECTROMAGNETIC SPECTRUM. *Edmund Optics* [online]. [cit. 2018-05-11]. Available from: `https://www.edmundoptics.com/resources/application-notes/optics/optics-101-level-1-theoretical-foundations/`

[46] HLAVIČKA, I. *Cyclotron resonance of Dirac electrons in bismuth selenide.* Brno, 2017. Master's thesis. Brno University of Technology. Faculty of Mechanical Engineering. Supervised by Ing. Miroslav Bartošík, PhD.

[47] MICHELSON, A. A. XXVIII. Visibility of interference-fringes in the focus of a telescope. *The London, Edinburgh, and Dublin Philosophical Magazine and Journal of Science* [online]. 2009, **31**(190), 256-259 [cit. 2018-05-31]. DOI: 10.1080/14786449108620101. ISSN 1941-5982. Available from: `https://www.tandfonline.com/doi/full/10.1080/14786449108620101`

[48] GRIFFITHS, P. R. a C. HOMES. UNITED STATES. DEPARTMENT OF ENERGY. OFFICE OF ENERGY RESEARCH. *INSTRUMENTATION FOR FAR INFRARED SPECTROSCOPY.* Brookhaven National Laboratory, 2001.

[49] KUZMANY, Hans. *Solid-State Spectroscopy* [online]. Berlin, Heidelberg: Springer Berlin Heidelberg, 2009 [cit. 2018-05-31]. ISBN 978-3-642-01478-9.

[50] *High magnetic field science and its application in the United States: current status and future directions.* Washington, D.C.: The National Academies Press, 2013. ISBN 978-0-309-28634-3.

[51] ORLITA, M., FAUGERAS, C., PLOCHOCKA, P., *et al.* Approaching the Dirac Point in High-Mobility Multilayer Epitaxial Graphene. *Physical Review Letters* [online]. 2008, **101**(26), - [cit. 2018-05-22]. DOI: 10.1103/PhysRevLett.101.267601. ISSN 0031-9007. Available from: `https://link.aps.org/doi/10.1103/PhysRevLett.101.267601`

[52] Facilities: Magneto-Optics. *Infrared Nano-Optics of Quantum Materials* [online]. [cit. 2018-03-25]. Available from: `http://infrared.ucsd.edu/facilities.html`

[53] PADILLA, W. J., LI, Z. Q., BURCH, K. S., *et al.* Broadband multi-interferometer spectroscopy in high magnetic fields: From THz to visible. *Review of Scientific Instruments* [online]. 2004, **75**(11), 4710-4717 [cit. 2018-05-11]. DOI: 10.1063/1.1805252. ISSN 0034-6748. Available from:`http://aip.scitation.org/doi/10.1063/1.1805252`

[54] Optical Spectroscopy: IR-spectroscopy laboratory. *ETH Zurich* [online]. [cit. 2018-03-25]. Available from: `http://www.spectro.ethz.ch/research/experimental-facilities.html`

[55] KUZMENKO, A. B. *Handedness resolved magneto-infrared spectroscopy of 2D and 3D Dirac materials* [online]. Winter School New Frontiers in 2D materials:

Approaches & Applications, 2017 [cit. 2018-03-25]. Available from: `http://old.ceitec.eu/alexey-kuzmenko/f34153`

[56] Division of Solid State Physics: Visible and IR magneto-optical system. *University of Warsaw* [online]. [cit. 2018-03-25]. Available from: `http://www.fuw.edu.pl/~zfcs/index.php/laboratoria-zfcs-po-2015r.html`

[57] Far infrared experiments: Far-infrared spectroscopy, Far infrared Fourier transform spectroscopy. *Radboud University: High Field Magnet Laboratory* [online]. [cit. 2018-05-11]. Available from: `http://www.ru.nl/hfml/facility/experimental/far-infrared/`

[58] MARX, R., MORO, F., DÖRFEL, M., *et al.* Spectroscopic determination of crystal field splittings in lanthanide double deckers. *Chemical Science* [online]. 2014, **5**(8), 3287- [cit. 2018-05-20]. DOI: 10.1039/c4sc00751d. ISSN 2041-6520. Available from: `http://xlink.rsc.org/?DOI=c4sc00751d`

[59] Protected Gold Mirrors: Features. *THORLABS* [online]. [cit. 2018-05-18]. Available from: `https://www.thorlabs.com/newgrouppage9.cfm?objectgroup_id=744`

[60] LABRIE, D., BOOTH, I. J., THEWALT, M. L. W., *et al.* Use of polypropylene film for infrared cryogenic windows. *Applied Optics* [online]. 1986, **25**(2), 171- [cit. 2018-05-12]. DOI: 10.1364/AO.25.000171. ISSN 0003-6935. Available from: `https://www.osapublishing.org/abstract.cfm?URI=ao-25-2-171`

[61] VERTEX 80/80v: VERTEX 80/80v FTIR spectrometers. *BRUKER* [online]. [cit. 2018-05-30]. Available from: `https://www.bruker.com/products/infrared-near-infrared-and-raman-spectroscopy/ft-ir-research-spectrometers/vertex-series/vertex-8080v/overview.html`

[62] MuMetal: About MuMetal. *MuShield* [online]. [cit. 2018-05-18]. Available from: `http://www.mumetal.com/about_mumetal.php`

[63] *VERTEX Series: Advanced Research FTIR Spectrometers* [online]. [cit. 2018-05-15]. Available from: `https://www.bruker.com/fileadmin/user_upload/8-PDF-Docs/OpticalSpectrospcopy/FT-IR/VERTEX/Brochures/VERTEXseries_Brochure_EN.pdf`

[64] Series 012 — Mini gate valve VATLOCK. *VAT* [online]. [cit. 2018-05-20]. Available from: `http://www.vatvalve.com/en/business/valves/catalog/A/012_1_V`

[65] OPUS Spectroscopy Software. *BRUKER* [online]. [cit. 2018-05-20]. Available from: `https://www.bruker.com/products/infrared-near-infrared-and-raman-spectroscopy/opus-spectroscopy-software.html`

[66] LOEWENSTEIN, E. V. and ENGELSRATH, A. Polarization properties of far infra-red beamsplitters. *Le Journal de Physique Colloques* [online]. 1967, **28**(C2), C2-153-C2-155 [cit. 2018-05-21]. DOI: 10.1051/jphyscol:1967228. ISSN 0449-1947. Available from: `http://www.edpsciences.org/10.1051/jphyscol:1967228`

List of Used Abbreviations

SMMs ...... Single-Molecule Magnets

FIR ...... Far-Infrared

2D 2-Dimensional

EPR ...... Electron Paramagnetic Resonance

FT-IR ...... Fourier-Transform Infrared

IPC ...... Institute of Physical Chemistry

CEITEC ...... Central European Institute of Technology

GHMFL ...... Grenoble High Magnetic Field Laboratory

CNRS ...... French National Center for Scientific Research (*Centre National de la Recherche Scientifique*)

MNMs ...... Molecular Nanomagnets

SIMs ...... Single-Ion Magnets

ZFS ...... Zero-Field Splitting

QTM ...... Quantum Tunneling of Magnetization

REEs ...... Rare Earth Elements

HDD ...... Hard Disk Drive

NMR ...... Nuclear Magnetic Resonance

INS ...... Inelastic Neutron Scattering

MCD ...... Magnetic Circular Dichroism

ESR ...... Electron Spin Resonance

CW-EPR ...... Continuous Wave Electron Paramagnetic Resonance

HF-EPR ...... High Frequency/Field Electron Paramagnetic Resonance

VTI ...... Variable Temperature Insert

MW ...... Microwave

QO ...... Quasi-Optics

IR ...... Infrared

FT-IR ...... Fourier-Transform Infrared

UV ...... Ultraviolet

FFT ...... Fast Fourier Transformation

NIR ...... Near-Infrared

MIR ...... Mid-Infrared

DTGS ...... Deuterium Triglycine Sulfate

MCT ...... Mercury Cadmium Telluride

3D 3-Dimensional

CAD ...... Computer-Aided Design

RFL ...... Reflected Focal Length

THz-FRaScan ...... THz Rapid Frequency Scans

OD ...... Outside Dimension

Appendix

CD with the INVENTOR drawings

Drawing No.	List of Drawing
1.00	OPTICAL SYSTEM
1.01	Guiding Tube
1.02	Front Plate
1.03	Housing
1.04	Parabolic Mirror
1.05	Mirror Mount
1.06	Back Plate
1.07	Adjusting Screw
1.08	Top Plate
1.09	Focusing Cone
1.10	Gate Valve
1.11	Gasket

Drawing No.	List of Drawing
2.00	TRANSMISSION PROBE
2.01	Outer Ring
2.02	Window
2.03	Inner Ring
2.04	Entrance Tube
2.05	Brass Tube 1
2.06	Brass Tube 2
2.07	Brass Tube 3
2.08	Probe Head
2.09	Probe Head Plate
2.10	Connector Plate
2.11	Probe holder Upper
2.12	Centering Plate
2.13	Squeezing Ring
2.14	Tube 1
2.15	Tube 2
2.16	Tube 3
2.17	Probe Holder 1, 2
2.18	Probe Cone
2.19	Probe Holder Bottom
2.20	Counterpart
2.21	Sample Holder
2.22	Sample Holder Plate
2.23	Pin
2.24	Sample Holder Rod
2.25	Rod Wheel
2.26	Rod Plate
2.27	Rod Ring
2.28	Extension
2.29	90° Mirror 1, 2
2.30	90° Mirror 3
2.31	Bolometer Plate
2.32	Window Tube 1
2.33	Window Tube 2
2.34	Window Ring